공학박사 학위논문

The Cost-Effective Thermal Control System of Small Lunar Landers and Rovers for Lunar Night Survival

소형 달착륙선과 로버의 달 밤기간 생존을 위한

비용 효율적 열제어 시스템

2020 년 8 월

서울대학교 대학원

기계항공공학부

이 장 준

Cost-Effective Thermal Control System of

Small Lunar Landers and Rovers for

Lunar Night Survival

A dissertation

submitted in partial fulfillment

of the requirements for the degree of

Doctor of Philosophy by

Jang-Joon Lee

Dissertation Advisor: Kyu-Hong Kim

School of Mechanical and Aerospace Engineering

Seoul National University

August 2020

Cost-Effective Thermal Control System of Small Lunar Landers and Rovers for Lunar Night Survival

소형 달착륙선과 로버의 달 밤기간 생존을 위한
비용 효율적 열제어 시스템

지도교수 김 규 홍

이 논문을 공학박사 학위논문으로 제출함
2020 년 8 월
서울대학교 대학원
기계항공공학부
이 장 준

이장준의 공학박사 학위논문을 인준함
2020 년 8 월

위 원 장	이 관 중	(인)
부위원장	김 규 홍	(인)
위 원	이 복 직	(인)
위 원	김 택 영	(인)
위 원	현 범 석	(인)

Abstract

Cost-Effective Thermal Control System of Small Lunar Landers and Rovers for Lunar Night Survival

<div align="right">

Jang-Joon Lee

School of Mechanical and Aerospace Engineering

The Graduate School

Seoul National University

</div>

A lunar day is equivalent to a month on the Earth. As a result, the daylight period of a lunar day is extremely hot due to two weeks of sunlight, and lunar nights are extremely cold due to the lack of sunlight for an equally long period. During lunar nights, lunar probes have no energy access from sunlight, and are required to withstand two weeks under extremely cold conditions.

Various devices have been proposed as solutions to ensure lunar landers and rovers are able to withstand two-week-long lunar nights. Certain methods utilize radioisotope heating units (RHU) and radioisotope thermoelectric generators (RTG), the heat source device and electric generator of lunar probes, respectively. In addition, radiator lids, which are thermal switches, have been applied for this purpose. Recently suggested ideas include thermal wadis, which are thermal storage devices, and devices that store energy from under the lunar surface during the lunar daytime.

ABSTRACT

As such thermal stability devices are accompanied with problems such as high costs, safety problems, or limitations in terms of weight or design, small lunar probes opt to forsake survival during the two-week-long lunar night and are instead designed for missions during the two-week daytime period.

This study proposes a new idea to enable small lunar landers and rovers to withstand the two-week-long lunar night: the multi-layer insulation (MLI) curtain system. The MLI curtain system uses devices such as a lid and RHU of the lunar lander to ensure lunar night survival, whereas the lunar rover enters into the shelter provided by the MLI curtain to survive during this period. This system has the advantage of being a relatively simplistic idea to ensure small lunar rovers can survive lunar nights, and is a low-cost solution.

In this study, the feasibility of the MLI curtain system was verified by conducting thermal design and thermal analysis according to general thermal design and analysis processes for spacecrafts. This produced a final result that met the thermal design requirements. Furthermore, to improve the feasibility of the MLI curtain system, the system is discussed not only from a thermal control standpoint, but also from structural, electric power, and software perspectives, resulting in ideas that could be suggested to improve the stability of the MLI curtain system. As a result, the MLI curtain system could prove to be a feasible and suitable idea to ensure the survival of small lunar rovers over long mission periods.

Keywords: Thermal Design, Thermal Analysis, Lunar Rover, Lunar Lander, Lunar Night Survival, MLI Curtain

Student Number: 2013-30208

Contents

CONTENTS

List of Tables

List of Figures

LIST OF FIGURES

Chapter 1. Introduction

1.1 History of Lunar Exploration Programs

Mankind's history in lunar exploration began with the Luna 1 of the former Soviet Union, which flew to the vicinity of the Earth's Moon in 1959. This was followed by Luna 2, which became the first spacecraft from Earth to contact the Moon's surface, and Luna 3 took the first photographic images of the far side of the Moon. Subsequent missions were taken to contact the Moon's surface or approach its orbit, and in 1966, the former Soviet Union succeeded in the first soft landing on the Moon's surface with Luna 9 [57].

Lunar exploration gained significant funding due to the Cold War between the United States and the former Soviet Union. The U.S. launched unmanned probes as the former Soviet Union were undertaking their lunar exploration missions, and in order to explore the potential of manned lunar missions, the U.S. undertook hard landing and soft landing programs referred to as the Ranger series and Surveyor series, respectively. Based on the lunar environment data obtained through these programs, the U.S. established the Apollo manned lunar exploration program. In 1968, the crew of the manned spacecraft Apollo 8 became the first humans to view the surface of the far side of the Moon upon entering the Moon's orbit, and in 1969, astronaut Neil Armstrong of the Apollo 11 crew became the first human in history to set foot on the Moon. The U.S. invested a considerable amount of money into the lunar exploration program to ensure successful breakthroughs within a short period of time, from hard landings on the Moon to manned missions. The

CHAPTER 1. Introduction

U.S. continued with its lunar exploration program, with the Apollo 17 mission in 1972 being the most recent manned mission to the Moon [57].

The lunar landing and exploration missions of the U.S. and the former Soviet Union were concluded in the mid-1970s, and funding were redirected to more challenging scientific missions to celestial bodies further away, such as Mars and Venus.

Entering the 1990s, Japan became the third nation to approach the vicinity of the Moon through its Hiten spacecraft [58], and this was followed by SELENE, which was launched for a mission in the Moon's orbit that lasted one year and eight months. SELENE concluded its mission as it collided with the Moon's surface as planned [59]. Japan had planned a SELENE 2 mission with a rover, although a specific development and launch schedule has yet to be decided.

The European Space Agency launched the SMART-1 lunar orbit satellite in 2003, which conducted a lunar observation mission [60].

China launched the lunar-orbiting spacecraft Chang'e 1 in 2007 for a lunar mission. In 2013, the lunar landing spacecraft Chang'e 3 was launched to explore the lunar surface, which was the first lunar surface exploration mission since the former Soviet Union's Luna 24 mission in 1976. In 2019, Chang'e 4 became the first spacecraft to land on the far side of the Moon [61].

India launched the lunar-orbiting spacecraft Chandrayaan-1 for a mission in 2008, which was followed by the launching of Chandrayaan-2 in 2019 for an observation mission from the Moon's orbit. The lunar surface lander and rover were unsuccessful in their missions [62].

The U.S. restarted its lunar exploration program in 1994 with the Clementine mission. Lunar Prospector, which was launched in 1998, completed its 1.5-year mission, and the Lunar Reconnaissance Orbiter launched in 2009 is still conducting its lunar observation mission as of 2020 as it was launched with sufficient fuel onboard [57].

CHAPTER 1. Introduction

1.2 Specifications of Unmanned Lunar Rovers

As the subject of this thesis is unmanned lunar rovers, we will review the main specifications of unmanned lunar rovers, excluding vehicles that were a part of the U.S. Apollo program. Table 1.1 summarizes the specifications of unmanned lunar rovers that have been manufactured and launched to date.

Table 1.1 Specifications of unmanned lunar rovers

Project Title (Spacecraft / Rover)	Luna 17 / Lunokhod 1 [37]	Luna 21 / Lunokhod 2 [37]	Chang'e-3 / Yutu [37]	Chang'e-4 / Yutu 2	Chandrayaan-2 /pragyan [38]
Mission Date	1970.11 ~ 1971.9	1973.1 ~ 1973.5	2013.12 ~ 2016.8	2019.1 ~	2019.09 ~ 2 weeks (fail)
Total Mass	5600 kg	4850 kg	3800 kg	-	3850 kg [37]
Lander Dry Mass	-	1814 kg	1200 kg	1200 kg [39]	1471 kg
Rover Mass	756 kg [7]	840kg	140 kg	140kg [39]	27 kg
Landing Site	38°N 35°W	26°N 30°E	44°N 20°W	46°S 178°E [40]	71°S 23°E [19]
Country	USSR	USSR	China	China	India
Survival Method of the Rover during Lunar Nights	RHU [8]	RHU [8]	RHU [41]	RHU	N/A

1.2.1 Lunokhod Series

Developed as part of the lunar program of the former Soviet Union, Lunokhod 1 was the first rover to successfully perform its mission on the lunar surface. An image of

Lunokhod 1 is shown in Figure 1.1 [49].

Figure 1.1 Mockup of Lunokhod 1 at the Memorial Museum of Astronautics [49]

In Figure 1.1, we can see the unfolded solar panel that supplies power to the rover. This is a configuration that involves charging the battery during the lunar daytime via sunlight to gather the power required for the rover's mission. The white surface on the top of Lunokhod 1 is a radiator that has a coating with low solar absorptivity and high infrared emissivity [7]. The material of the radiator coating is presumed to be white paint, which serves to dissipate waste heat inside the rover to the outside during hot lunar days. As solar heat is absent during lunar nights, the rover is exposed to an extremely cold surrounding environment during these periods. For this reason, Lunokhod 1's solar panel

(lid) was folded to prevent heat loss. Moreover, Lunokhod 1 was equipped with an RHU [8], which supplies heat during lunar nights to ensure all parts of the rover were controlled within the allowable temperature, allowing the rover to survive such cold conditions. Lunokhod 1 was a large rover with a mass of 756 kg, and the rover itself could be equipped with a lid opening and closing system, RHUs, and a large-capacity battery.

Figure 1.2 [45] shows a mockup of Lunokhod 2. The specifications of Lunokhod 2 were similar to Lunokhod 1, and both had the same thermal design.
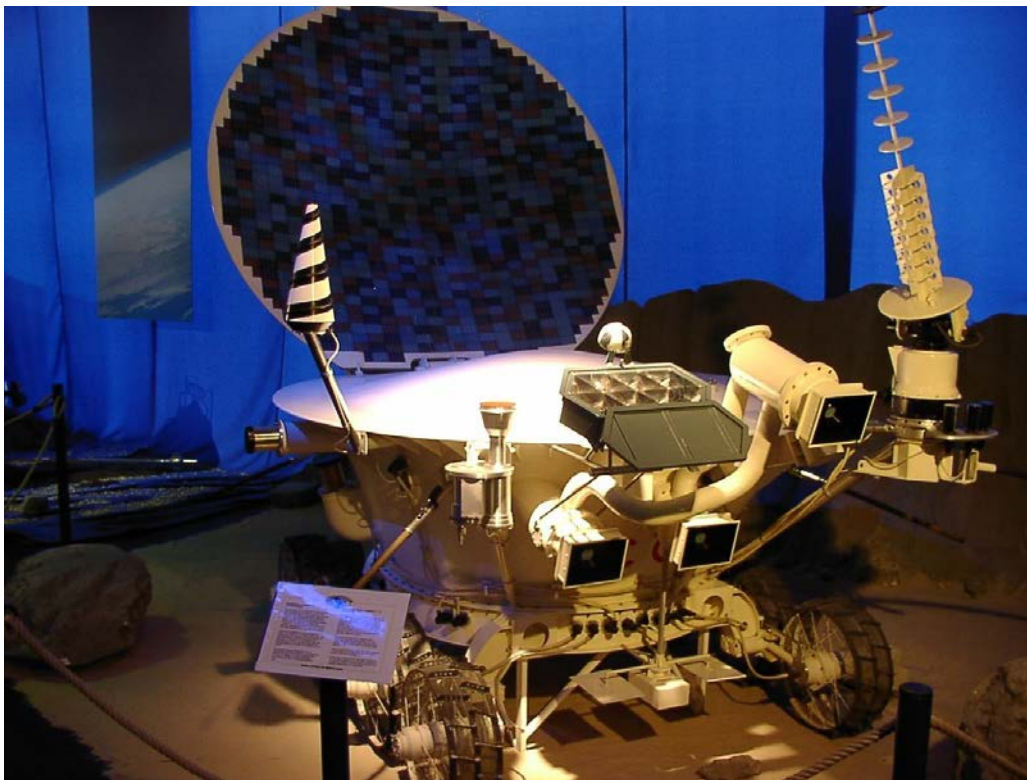
Figure 1.2 Mockup of Lunokhod 2 at the Memorial Museum of Astronautics [45]

1.2.2 Yutu Series

The first lunar lander launched by China, Chang'e 3, was equipped with a Yutu rover. Figure 1.3 [46] shows the shape of Yutu through a photograph taken by Chang'e 3 during actual Yutu activity on the lunar surface.
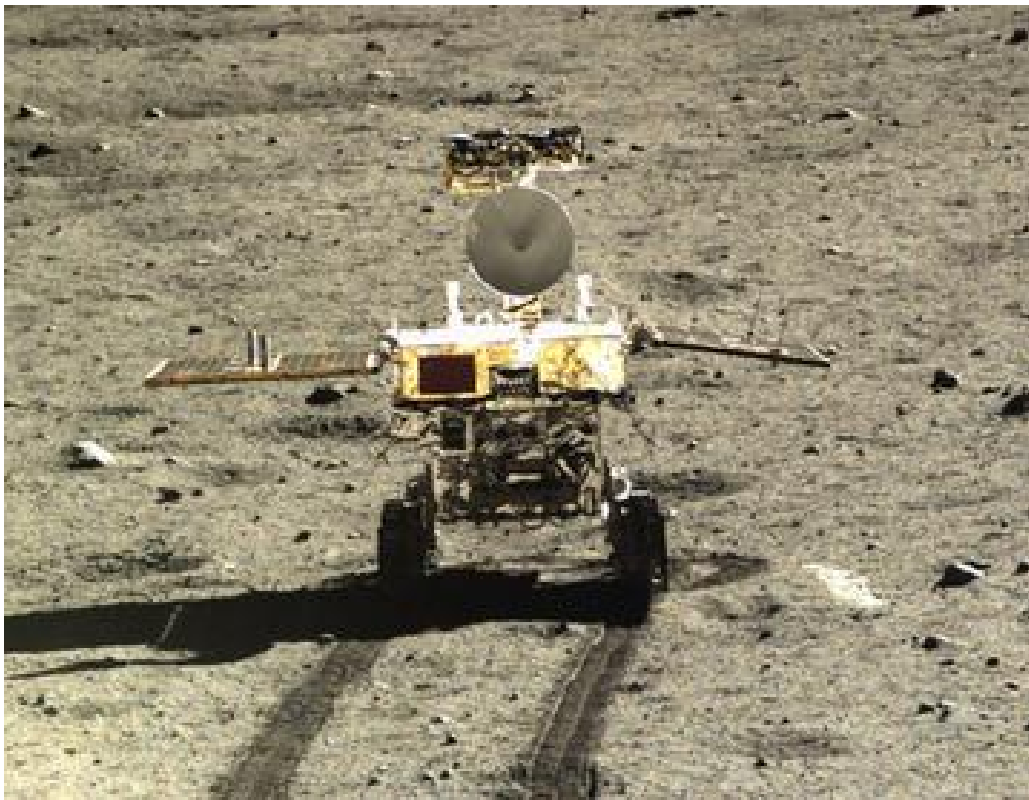
Figure 1.3 Yutu rover on the lunar surface, photographed by the Chang'e 3 lander [46]

The Yutu rover had a mass of 140kg [37] and landed with the lunar lander Chang'e 3. Originally, Yutu was designed with a mission life of three months, but the rover managed to last 31 months.

In Figure 1.3, we can see that Yutu's solar panels are facing away from the lunar

surface. In addition, Yutu was equipped with RHUs to survive during lunar nights [41]. As in the case of the Lunokhod series, Yutu is presumed to be designed with a radiator to release the rover's waste heat in the upward direction of the body. It has yet to be confirmed whether the solar panels were used as lids to cover the radiator during lunar nights.

Yutu 2 is a rover that was mounted on the lunar lander Chang'e 4 launched in January 2019. Yutu 2 is almost identical in size and mass as Yutu 1, but the former's mission area is on the far side of the Moon from the Earth. Yutu 2 was originally designed for a mission life of three months, but it has survived beyond this period and is still performing its mission as of May 2020. Yutu 2 is also equipped with RHUs like Yutu 1 to survive during lunar nights, and is presumed to have the same thermal design as Yutu 1.

1.2.3 Pragyan

Chandrayaan 2 was launched in September 2019 and consisted of a lunar orbiter, the lunar lander Vikram, and the rover Pragyan. Vikram and Pragyan were originally planned to perform a mission for 0.5 lunar days (14 days on Earth) [47], but Vikram failed to perform a soft landing on the lunar surface and could not achieve its mission. The Vikram lander had a mass of 1471 kg and the Pragyan rover weighed 27 kg [47].

Vikram and Pragyan were able to generate electrical power through installed solar cells [47]. Both could only survive for a short period of two weeks, which is equivalent to the period of lunar daytime. It is believed that survival was not possible during lunar nights as no RHUs were installed.

1.3 Thesis Objective and Proposal

As described in the previous section, lunar surface exploration projects, which halted during the mid-1970s, have recently seen a revival in countries like China, Japan, India, and the United States. The Republic of Korea also aims to join the Moon exploration competition by setting a target to launch a test lunar orbiter in 2021 and a lunar lander in 2030.

Spacecraft development is a costly endeavor. Commercial Earth observation satellites amount to hundreds of millions of dollars, and thus lunar exploration projects are promoted at the national level. A factor that greatly influences the cost of spacecraft development is the mass of the spacecraft. Previous studies on the correlation between spacecraft mass and cost [26], [50] have shown that the overall mission cost significantly increases as the spacecraft mass increases. The approximate relationship between satellite mass and cost was derived by M. Mirshams et al.[26]: the mass and cost relationship for scientific satellites with masses ranging from 10 kg to 1000 kg is given by Eq. 1.1 [26].

$$Y = 0.0008 * x^{2.2459} \quad\quad\quad\quad (Eq.\ 1.1)$$

In Eq. 1.1, the unit of x is kg and the unit of Y is M\$. By using Eq. 1.1 to calculate the mass to cost ratios of a 300kg satellite and a 900kg satellite, we can determine that the 900kg satellite, despite having three times the mass of the 300kg satellite, results in costs 11.8 times greater.

CHAPTER 1. Introduction

Although Eq. 1.1 is a satellite formula, the fact that the development cost of a lunar lander and rover increases as the mass increases remains the same. Therefore, the purpose of this thesis is to determine a means of achieving long mission times even with small mass rovers, which would help save the cost of lunar exploration projects to suit the situation of Korea.

The subject of this study are small rovers with a mass range of 20~30 kg. For small lander and rover programs, it is difficult to set up an RHU or RTG system in small rovers. For this reason, small rovers have not been able to survive lunar nights until recently. As shown in Table 1.1, rovers that perform long-term missions exceeding two weeks have masses of at least 100 kg. In contrast, the 27 kg small rover that was loaded in Chandrayaan-2[38] was designed for short-term missions of less than two weeks.

This study proposes a lunar night survival method involving an MLI curtain system that enables small rovers of 20~30kg to perform long-term missions. The system can be summarized as a small rover without an RHU that performs mission tasks during the daytime and continues to survive in an MLI curtain shelter that is part of the lunar lander during lunar nights. The rover can perform short missions even during lunar nights according to power margins, and it can perform missions again upon the return of the lunar day. In order to prove the feasibility of the MLI curtain system for lunar night survival, this study introduces a thermal model of a lunar lander and a rover in a lunar thermal environment and presents the analysis results.

Chapter 2. Thermal Design of Lunar Exploration Vehicles

2.1 General Spacecraft Thermal Design Process

Spacecraft thermal design is a complex and iterative process that constantly requires repetition and review to conform with a wide array of other systems. Hence, the thermal design process only concludes with the launch of the spacecraft. Spacecraft thermal design can be largely divided into the thermal hardware design process and the thermal analysis process with the goal of satisfying system requirements. The two processes exchange input information with each other and undergo an iteration process of readjustment through the sharing of design results.

The design of a spacecraft should adhere to the intended mission. For example, a cube satellite on a month-long mission does not require advanced components for space radiation. On the other hand, large geostationary satellites with mission durations exceeding 10 years require significant amounts of fuel to maintain orbit and attitude. In the same manner, the thermal design of a spacecraft should be in accordance with its mission duration, mission environment, and payload characteristics.

In spacecraft thermal design, input variables are required for thermal analysis. Environmental variables require information such as the satellite's external shape, orbit configuration, altitude information, and mission life. In addition, the process requires the following information: the thermal properties of components, unit allocation information, unit operating time, heat dissipation, surface optical properties, external surface finishes, MLI (Multi-Layer Insulation) material, heater capacity, and the location and size of the

11

radiator. Using this information, a geometric model for thermal analysis can be developed.
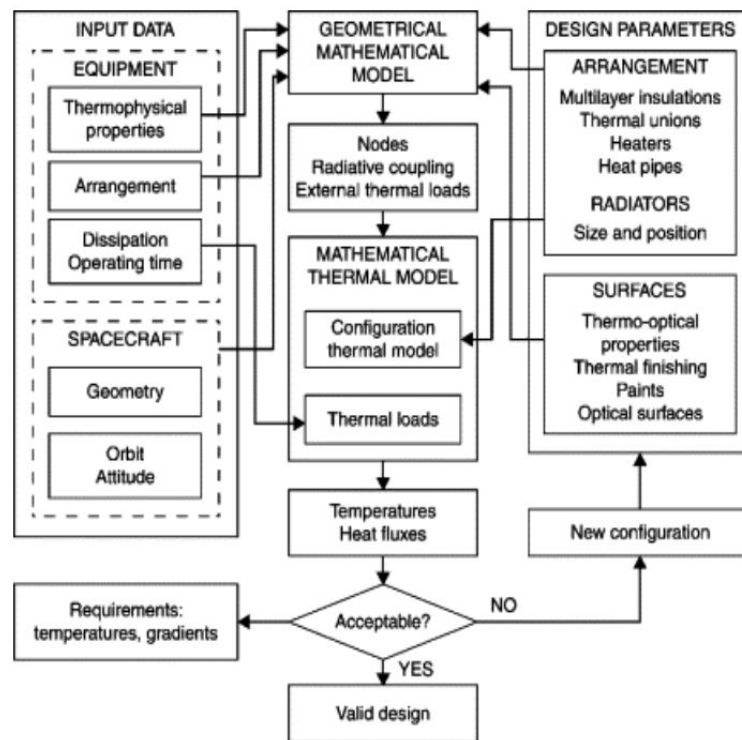
Figure 2.1 Design process flowchart for thermal control subsystems [1]

Once the geometric model is constructed, a thermal mathematical model can be developed by discretizing the geometric model, calculating the radiative heat exchange coefficient and the external heat inflow. With the completion of the thermal mathematical model, it is possible to calculate the expected heat flux and temperature of the spacecraft through simulations of mission scenario cases. If the derived thermal analysis results

meet the temperature requirements of all components, the thermal design is deemed complete. Conversely, if the thermal analysis results do not meet the temperature requirements, a new design is derived through the thermal control hardware design process, and the iteration process is again performed for thermal analysis to determine if the new results meet the temperature requirements. This process is illustrated in Figure 2.1 [1].

A spacecraft cannot modify its configuration after leaving Earth. For this reason, in order to increase the reliability of the spacecraft, the thermal control subsystem should be designed with the assumption of worst-case conditions and should include redundancy designs, and a design with uncertainty margins. In other words, the thermal analysis in the thermal design process should be performed with the potentially coldest and hottest conditions, and all thermal control hardware should have redundancies.

The resource for a spacecraft's thermal control system is its power demand. If the uncertainty margin of the thermal control system is too large, the power demand of the spacecraft increases. This leads to an increase in spacecraft development costs due to increases in solar panel size, battery capacity, and power distribution channel. Therefore, it is important to properly set the uncertainty margin of the thermal control system.

Figure 2.2 shows a guideline for the design temperature of a thermal control system proposed by the European Space Agency [13].
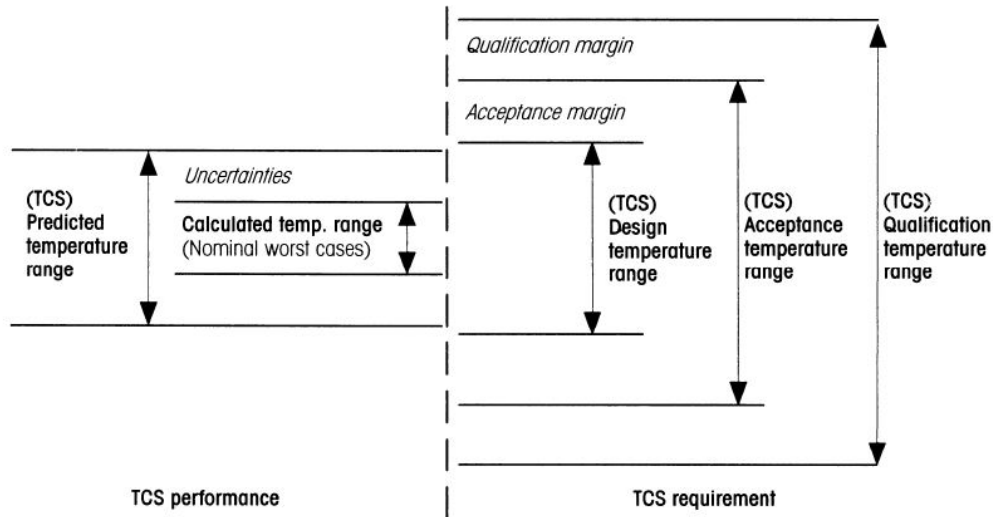
Figure 2.2 Temperature definitions for thermal control systems [13]

In Figure 2.2, the predicted temperature range is derived from the calculated temperature range by including the uncertainty of the temperature calculation range, assuming worst cases. As such, the calculated temperature range should be encompassed within the design temperature range. Manufacturers of spacecraft equipment are required to develop their equipment with an appropriate acceptance margin from the design temperature range for flight models. In the case of qualification models, in addition to the acceptance temperature range, verifications are required for the temperature range in which the qualification margins are secured.

It is necessary to verify the derived thermal design results, and the final verification is usually performed through the thermal vacuum test of the flight model. Figure 2.3 shows a photograph of the satellite thermal vacuum test.
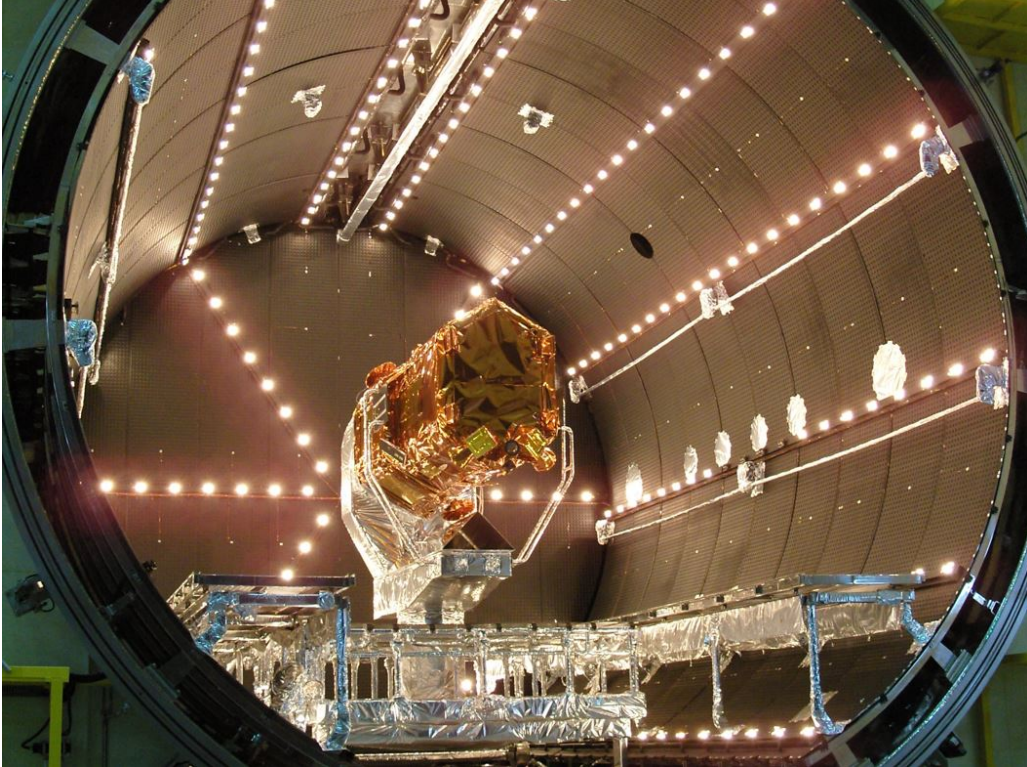
Figure 2.3 Satellite thermal vacuum test

By comparing the temperature results obtained from the thermal vacuum test with the thermal analysis results, the correlation process of the thermal mathematical model is performed. As a result, the thermal control hardware is rearranged according the corrected thermal analysis model. Through this process, the final satellite shape is determined. The spacecraft thermal control system design process is concluded with the design of the final shape of the MLI after the spacecraft is combined with the launch platform for launch. The final confirmation of the spacecraft's thermal design results is verified through telemetry, which is sent from the spacecraft to the Earth's station.

2.2 Thermal Environment of the Moon

A conceptual diagram of the orbital shape of the Sun, Earth, and Moon is shown in Figure 2.4.
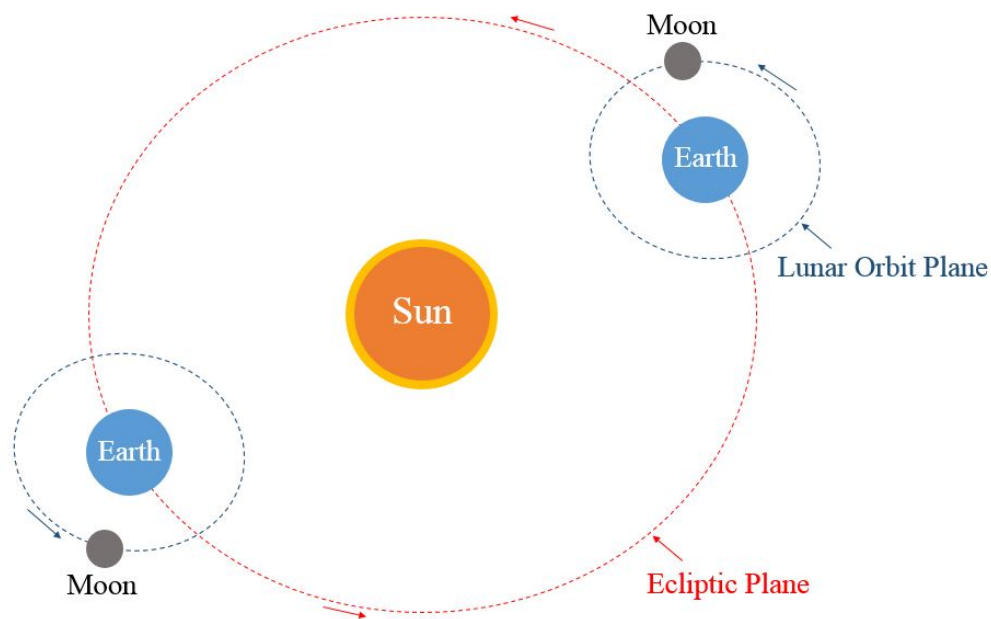
Figure 2.4 Relative motion of the Earth and Moon

The Moon is constantly influenced by the Earth's gravity, and always faces the Earth with the same side. The Moon's orbit and rotation cycle are the same length, and a day on the Moon relative to the Sun is equivalent to 29.5 Earth days. The daytime period on the Moon corresponds to approximately two weeks, which is half the full day period. Likewise, the remaining two weeks corresponds to the night period of the Moon.

The ecliptic plane of the Earth's orbit around the Sun and the lunar orbit plane of the

Moon's orbit around the Earth do not lie in the same plane. Just as there is a constant angle between the Earth's rotational axis and its orbital plane, there is also a constant angle between the Moon's rotational axis and its orbital plane. Figure 2.5 shows a conceptual diagram of the relative relationship between the Moon's orbital plane and its axis of rotation [54].
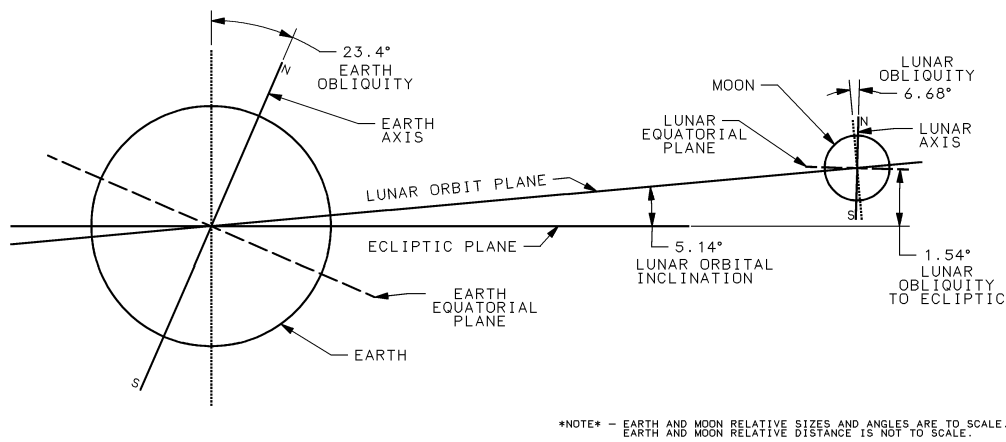
Figure 2.5 Diagram of the Moon's orbit with respect to the Earth [54]

As illustrated in Figure 2.5, an angle of 5.14° exists between the orbital plane of the Moon and the orbital plane of the Earth, and an angle of 6.68° exists between the axis of rotation and orbital plane of the Moon. This indicates that the Moon's equator only deviates from its orbital plane by 1.54°. This means that even if thermal analysis is performed by setting the angle between the axis of rotation and ecliptic plane of the Moon as 88.46° ≅ 90°, the analysis results will exhibit little variation.

On the other hand, due to the Moon lacking any form of atmosphere like the Earth's

atmosphere, there is no absorption layer for incident sunlight. Furthermore, the absence of an atmosphere also means there is no convection, and thus energy exchange does not occur between the surfaces of the Moon. As a result, the temperature of the Moon's surface is extremely hot in the area exposed to sunlight, and the temperature of the Moon's surface exhibits a cosine distribution according to the angle of incidence of sunlight [13]. Conversely, the temperature of the opposite surface where sunlight does not enter becomes extremely cold.
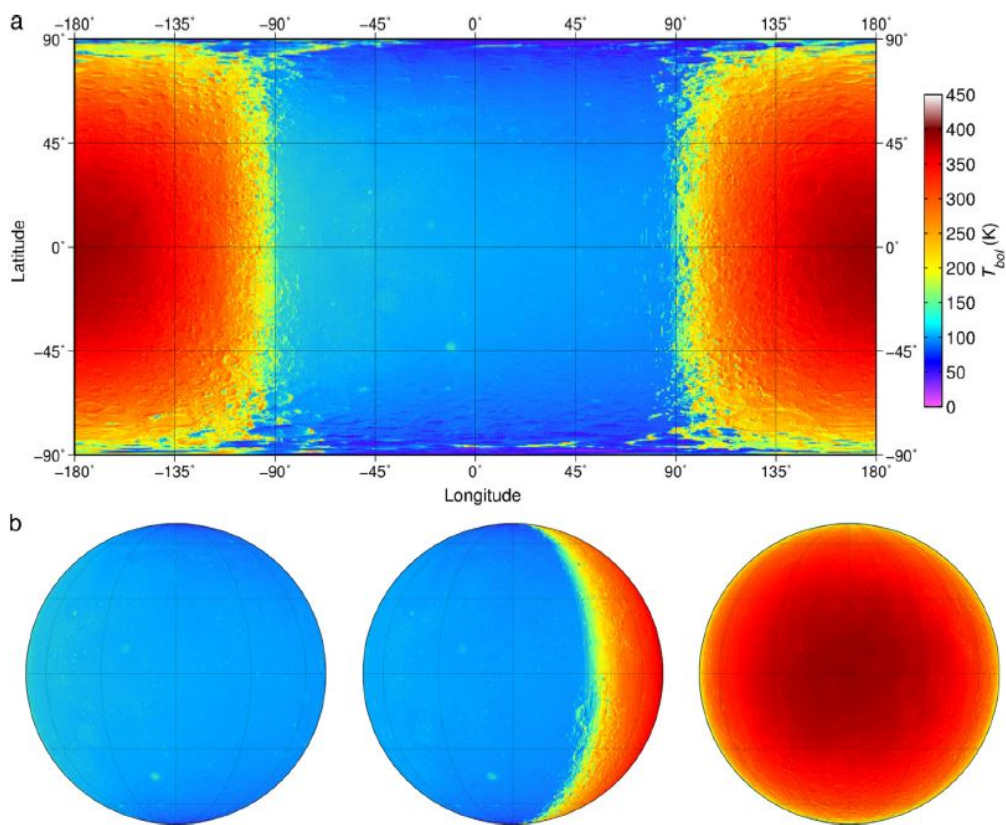
Figure 2.6 Surface temperatures of the Moon expressed in (a) cylindrical equidistant projection and (b) orthographic projection (subsolar longitude at 180˚, 120˚, and 0˚)[24]

Measurement values of the surface temperature of the Moon include estimated values based on the data measured by Apollo 11 to 13 as well as results of recent studies based on the measured values of LRO (Lunar Reconnaissance Orbiter) satellites [24]. The figure showing the surface temperature of the Moon in Figure 2.6 is cited in Ref. [24].

According to Figure 2.6, the maximum temperature of the Moon's surface that is exposed to sunlight reaches 400K or higher, and the temperature of the Moon's surface where sunlight does not enter is below 100K. As such, it is clear that the lunar surface exhibits extreme temperature variations.

Furthermore, it is also known from the experimental results of Apollo 11 that the substances that comprise the lunar surface have exceptionally low heat transfer coefficients and heat capacities [2]. Therefore, even during lunar daytime periods, if a shadow is generated by an object, the temperature under the shade remains low in contrast to the surrounding hot temperature.

2.3 Thermal Hardware of Lunar Exploration Vehicles

This section describes the thermal control hardware to be applied to lunar landers and rovers that will be discussed in this thesis.

2.3.1 MLI (Multi-Layer Insulation)

MLI, which can be viewed as a spacecraft's clothing, refers to multiple layers of metal with low emissivity. MLI is used as insulation in space. Figure 2.7 explains the principle of MLI.
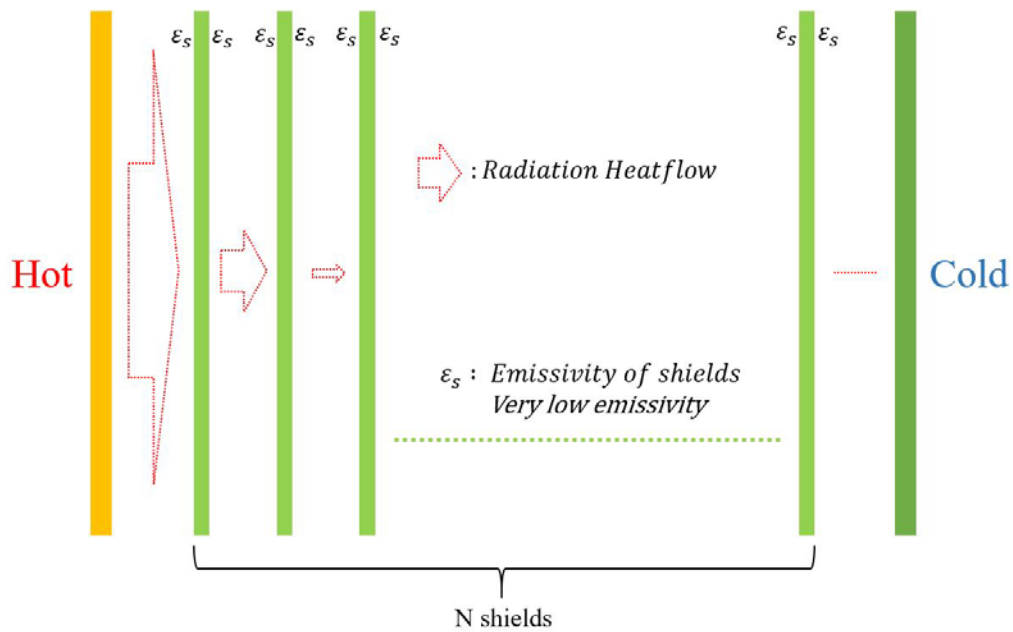
Figure 2.7 Heat flow configuration of MLI

The principle of MLI is based on the fact that the only heat transfer paths in outer space are conduction and radiation, as convection is not possible. MLI cuts the conduction path by placing spacers between the multiple layers of metal. MLI also blocks radiation by placing a layer of metal with low emissivity in the heat transfer path. According to Figure 2.7, heat transfer occurs through radiation from the hot side to the cold side. Shields located in the middle region are made of metal with low emissivity, so the shields reflect most of the radiant energy and absorb only a small amount. As the radiant energy passes through the shields across several stages, the amount of energy transferred rapidly decreases, and almost no energy reaches the cold side. The temperature of the hot and cold sides of the MLI can be continuously maintained at hot and cold states, respectively.

In MLIs, the shield material of choice is aluminum (VDA, Vacuum Deposited Aluminum) with an emissivity value of 0.03. In addition, polyimide or polyester materials are used to maintain the shape of aluminum in MLIs. As the layer constituting the MLI is very thin, MLIs can be easily manufactured with a 3D shape in addition to atypical shapes. Figure 2.8, Figure 2.9 [51], and Figure 2.10 introduce design examples and actual appearances of MLIs.
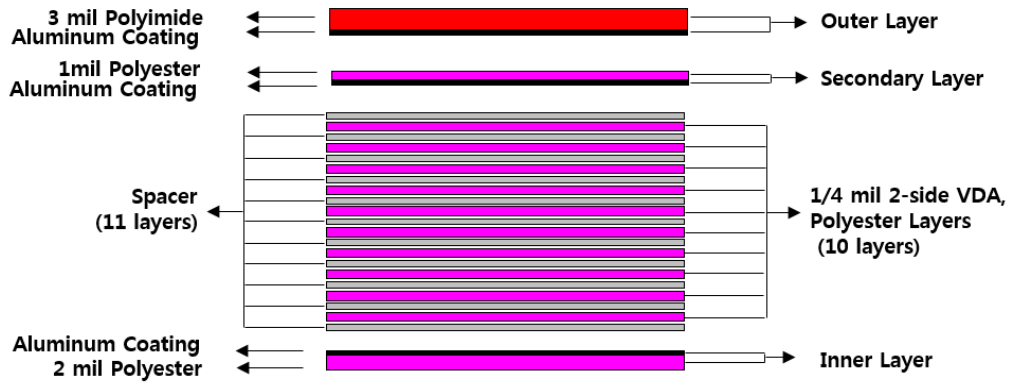
Figure 2.8 Example of MLI Layer Design

Figure 2.9 Inner Configuration of an MLI [51]

Figure 2.10 MLI installation on a satellite

2.3.2 SSM (Second Surface Mirror)

Whereas MLIs insulate space vehicles from outer space, an SSM acts as a channel for radiating the spacecraft's waste heat into space. SSMs are mounted on the outer panel of a spacecraft and are applied to a fixed area. SSMs are also referred to as optical solar radiators (OSR). The ultimate heat sink of a spacecraft is deep space, which approaches the absolute temperature of 0K. SSMs achieve heat dissipation through a radiation mechanism. To explain the basic principle of radiative heat transfer in radiators, we begin with the equation for the radiant energy of a black body, shown in Eq. 2.1 [3].

CHAPTER 2. Thermal Design of Lunar Exploration Vehicles

$$E_{b\lambda}(\lambda, T) = \frac{C_1}{\lambda^5[\exp(C_2/\lambda T)-1]} \ (W/m^2 \cdot \mu m) \hspace{2cm} \text{(Eq. 2.1)}$$

where C_1= 3.742 x 10^8 W·$\mu m^4/m^2$ and C_2= 1.439 x 10^4 μm·K. Additionally, T is the absolute temperature of the surface and λ is the wavelength of the emitted radiation. The variation in spectral black body emissive power according to wavelength is plotted in Figure 2.11 [3].
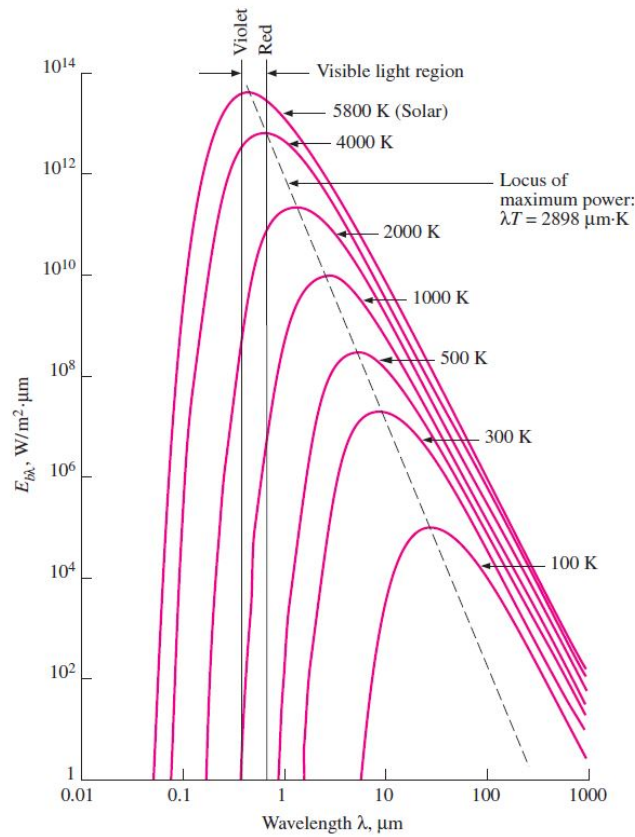
Figure 2.11 Emissive power according to wavelength for various temperatures [3]

24

Figure 2.11 shows the radiant energy of a black body; the radiant energy of an actual object is lower than the value shown in the graph. In Figure 2.11, the surface of the Sun, which corresponds to temperatures of 5800K, emits various forms of radiation in the ultraviolet, visible, and infrared regions, whereas a spacecraft corresponding to temperatures of 300K emits energy only in the infrared region.

Actual objects are generally not black bodies and exhibit highly irregular patterns of radiant energy. However, an actual object with an irregular radiation pattern can be assumed to be a gray surface with a radiation pattern similar to a black body. Emissivity is the ratio of energy emitted by a gray surface to the energy emitted by a black body. Figure 2.12 shows examples of radiation patterns of a real surface and a gray surface [3].
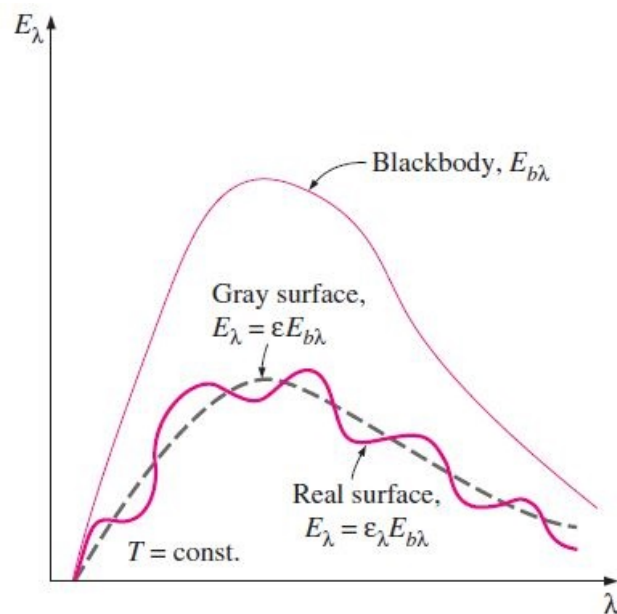
Figure 2.12 Emissivity power of a real surface, a black body, and a gray surface [3]

In Figure 2.12, the real surface can be assumed to be a gray surface, and the emissivity (ε) concept can be introduced to express the amount of radiant energy of an object. As shown in Figure 2.12, the surface radiation energy of a real object (E_λ) is assumed to be a gray body and can be expressed as Eq. 2.2. Here, emissivity (ε) has a range of $0 < \varepsilon < 1$ and $E_{b\lambda}$ is black body energy.

$$E_\lambda = \varepsilon \, E_{b\lambda} \qquad\qquad\qquad\qquad \text{(Eq. 2.2)}$$

The radiant energy emitted by object A is a function of the wavelength corresponding to the temperature of object A's surface. However, the incident energy on object A is a function of the wavelength corresponding to the surface temperature of object B, which emits energy. For this reason, the radiator of a spacecraft must have high emissivity (ε) in the infrared region, which is the wavelength region for waste heat emission, and low absorption (α) in the wavelength region of solar heat inflow. The main performance index for a radiator is the ratio α/ε, with a lower index value corresponding to better performance.

White paint has a solar absorption value of approximately 0.2 and a surface emissivity value of 0.9. Therefore, it can serve as an excellent radiator with an α/ε ratio of 0.45. However, an SSM with an α/ε ratio half the value of white paint is still superior as a radiator. To explain, Figure 2.13 illustrates the principle of SSMs [2].
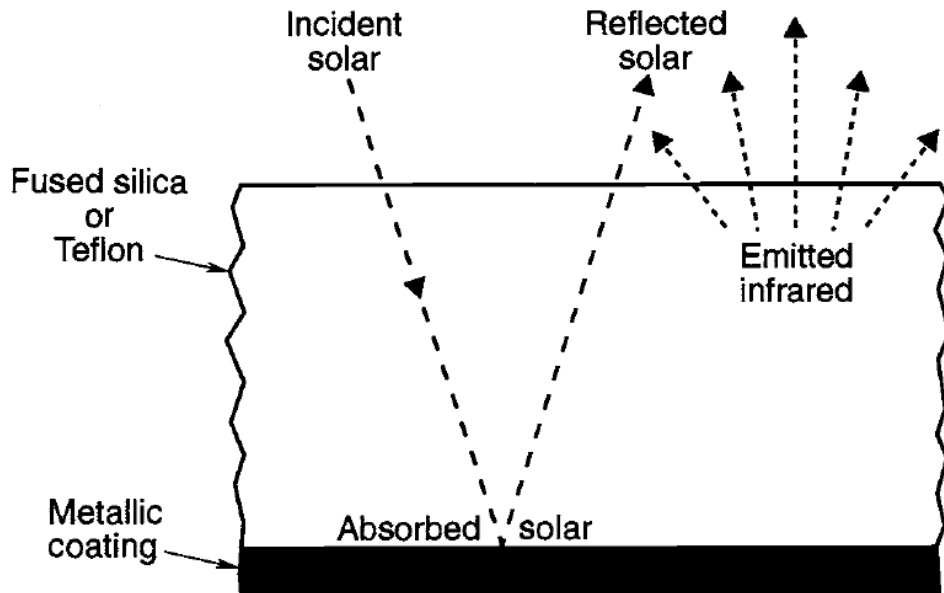
Figure 2.13 Energy path of Second-Surface Mirror [2]

An SSM is a device that applies a metal coating to transparent materials such as Teflon. Metal materials have low solar absorption and low surface emissivity. The incident sunlight from the outside passes through the transparent material such as Teflon and is reflected off the metal surface. The outer layer of an SSM, being comprised of Teflon, allows infrared heat radiation to pass through. Due to the low solar absorptivity of metals, most of the solar energy is reflected back to the outside. This, in addition to the relatively high emissivity of the outer Teflon surface, allows SSMs to have low solar absorptivity and high emissivity. SSMs are shaped like a mirror and are the most notable form of spacecraft radiators. Figure 2.14 shows an actual SSM mounted on a spacecraft structure.
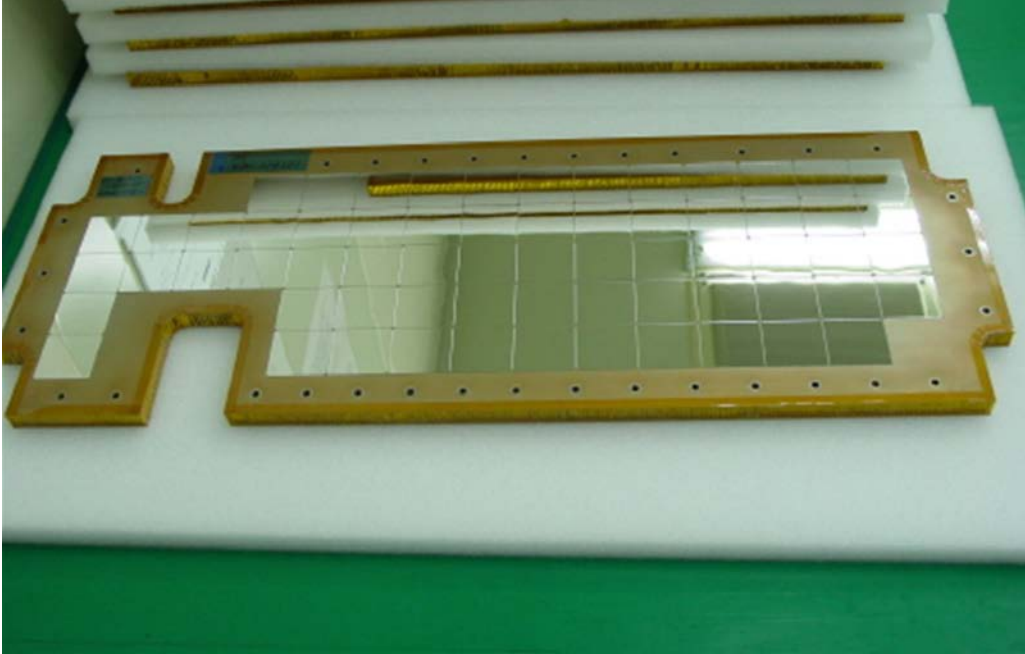
Figure 2.14 An SSM installed on a spacecraft panel

2.3.3 RTGs and RHUs

Radioisotope thermoelectric generators (RTGs) provide electrical energy to spacecraft on missions that do not depend on sunlight. For example, it was applied to the Viking lander that operated on the surface of Mars as well as Voyager that undertakes missions outside the Solar System. RTGs supply energy by converting thermal energy generated through nuclear fission into electrical energy. RTGs have the advantage of being able to produce energy even in the absence of sunlight. However, there are several disadvantages to the technology, such as high development and production costs, safety problems due to radioactivity concerns, and decreased power production as nuclear fission progresses. Furthermore, the operation of an RTG cannot be stopped even when

it is desirable to cease the generator, and a separate device is required to dissipate the waste heat. In addition, RTGs generate energy with poor efficiency levels of approximately 10%, meaning 90% of the energy is discarded into deep space through fins [4]. Figure 2.15 [52] illustrates an example of an RTG and its configuration.
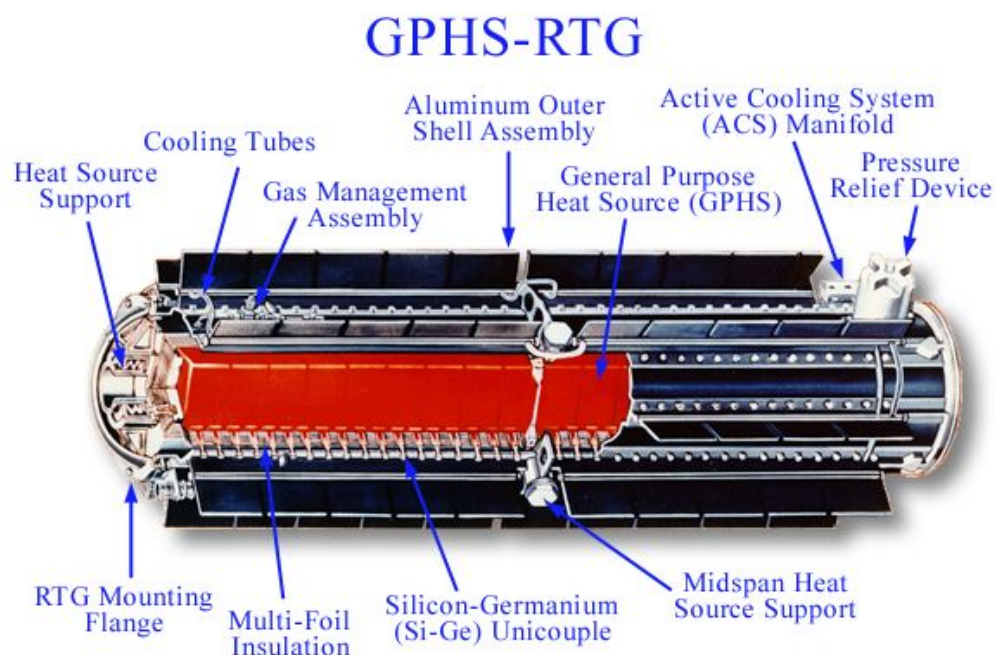
Figure 2.15 Configuration of a GPHS RTG [52]

Due to the low efficiency and high cost of RTGs, radioisotope heater units (RHUs) were developed as an alternative. RHUs omit the process of converting heat into electricity in RTGs and use heat from nuclear fission instead of an electric resistance heater [2]. RHUs, like RTGs, have disadvantages arising from fission and radioactivity. On the other hand, RHUs have advantages in terms of the relatively low cost and

relatively high efficiency compared to RTGs. RHUs can be developed in small sizes and can supply heat by being installed in multiple positions according to the thermal design. Figure 2.16 shows an example of an RHU and its configuration [2].
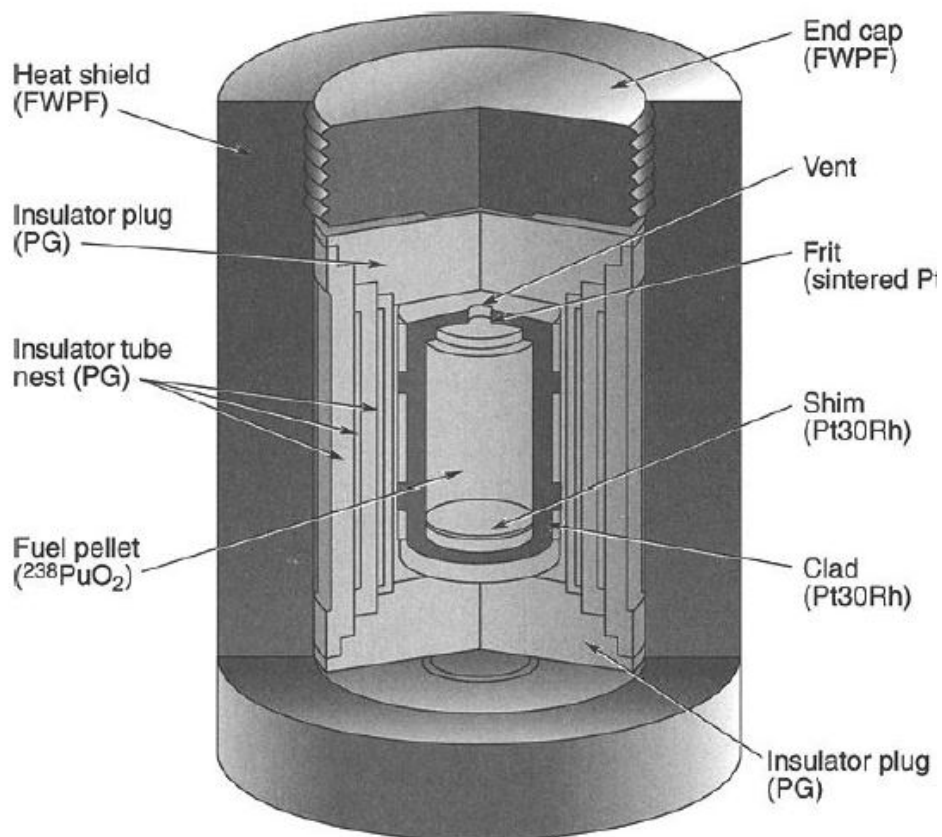
Figure 2.16 Configuration of a radioisotope heater unit (RHU) [2]

2.4 Thermal Design of Lunar Landers and Rovers

As seen in Section 2.2, the lunar surface exhibits extremely high temperatures of approximately 400K during the day, and extremely low temperatures of approximately 100K during the night. In general, a spacecraft unit is developed with an allowable temperature range of approximately 250K ~ 330K. Due to the vast difference in lunar surface temperatures throughout a day on the Moon, the spacecraft's temperature could increase beyond the allowable high temperature limit during the daytime, or decrease below the allowable low temperature limit during the nighttime. Therefore, if the Moon surface and the space vehicle exhibit strong thermal coupling, it will become exceptionally difficult to control the temperature of the spacecraft within the allowable temperature range. For this reason, it is necessary to thermally separate the spacecraft from the lunar surface, and it is desirable for landers and rovers to direct the radiator in the opposite direction to the lunar surface to reduce thermal coupling with the lunar surface. In the case of the Lunokhod series, the Yutu series, and Pragyan discussed in Section 1.2, radiators are placed on top of the rover.

The duration of missions on the lunar surface also affects the thermal design of lunar landers and rovers. The Lunokhod series and Yutu series were required to survive during the daytime and nighttime phases of the Moon due to mission periods exceeding two weeks. In order to survive during lunar nights, it is necessary to minimize the leakage of heat to the outside, and a heat source should be prepared to maintain the units within the allowable temperature range during the night period. The Lunokhod series used RHUs

31

as heat sources for survival during lunar nights and minimized heat leakage by covering the radiator with a lid. The Yutu series vehicles were also thermally designed to survive lunar nights using RHUs as heat sources. As Pragyan was purposed for a mission lasting two weeks, it was designed to survive only during the lunar daytime. Therefore, heat sources such as RHUs necessary for survival during lunar nighttime periods were not considered.

Lunar night survival is a task that encompasses significant challenges and one that is essential if lunar landers and rovers are to perform missions longer than two weeks. Although heat sources are essential for lunar night survival, the inclusion of such technology can lead to significantly higher costs and greater technical challenges. In Chapter 3, several methods and features of lunar night survival are described in detail.

Chapter 3. Methods of Lunar Night Survival

3.1 Nuclear Energy

Lunar landers and rovers that perform missions exceeding a month (one lunar day) are required to survive in a temperature environment of -190℃ for two weeks without any supply of heat from external heat sources such as solar heat. As lunar landers or rovers cannot survive without a heat source during this period, most lunar exploration programs employ RHU (Radioisotope Heating Units) or RTG (Radioisotope Thermoelectric Generators)[8] for lunar night survival, as described in Table 1.1.

As of the time of this writing, survival methods for lunar nights that have been successfully proven still use RHU or RTG systems. Table 1.1 summarizes the specifications of unmanned rovers and landers, not including US manned mission, to compare with the subject of this study. Table 1.1 shows that all past unmanned lunar surface exploration missions involved the use of RHU or RTG systems.

3.2 Lid System

As discussed in Section 2.1, the thermal design of a spacecraft is based on the worst possible thermal environment conditions. Under the potentially hottest conditions that a spacecraft can be subjected to, the thermal design should adjust the radiator size to ensure the temperature of spacecraft components do not exceed the maximum allowable temperature. Additionally, thermal design processes are undertaken to determine the capacity of heaters within the power budget limit allocated to the thermal control system, ensuring that the determined spacecraft shape can maintain the minimum allowable temperature under the potentially coldest conditions.

In spacecraft such as lunar landers, a lid can be used to maintain an open configuration under hot conditions to release waste heat from the spacecraft. Moreover, the lid can also maintain a closed configuration to prevent temperature drops in the spacecraft under cold conditions. In the case of most spacecraft, if the radiator is increased to lower the temperature of the spacecraft under hot conditions, this is inevitably accompanied by an increase in heater power consumption under cold conditions. However, the use of a lid system can suppress the latter increase in heater power consumption.

In the case of satellites, it is difficult to implement a lid system due to the changes in center of gravity caused by the operation of the lid system. Furthermore, the lid could give rise to field-of-view (FOV) interference that affects the communication antenna. On the other hand, in the case of lunar landers, the usefulness of lid systems was proved

through the Lunokhod series [37]. As a result, lid systems can play a significant role in reducing the heater power consumption of lunar landers.

3.3 Feasible Proposals

With concerns of RHU and RTG regarding radioactive contamination, several efforts are being made to find other methods for lunar night survival. R. Balasubramaniam et al.[9] proposed the Thermal Wadis to survive lunar nights without RHU or RTG. Thermal Wadis is a device that maintains the temperature of rovers during lunar nights by absorbing heat from the sun during the daytime of the Moon by installing an object of high capacity and low thermal conductivity on the surface of the Moon. Thermal Wadis accumulates solar heat during the daytime of the Moon, and employs heat shielding to limit heat radiation to space during the lunar night. The difficulty of this method involves the requirement of complex and heavy systems to implement Wadis. Figure 3.1 [9] shows the conceptual diagram of Thermal Wadis.
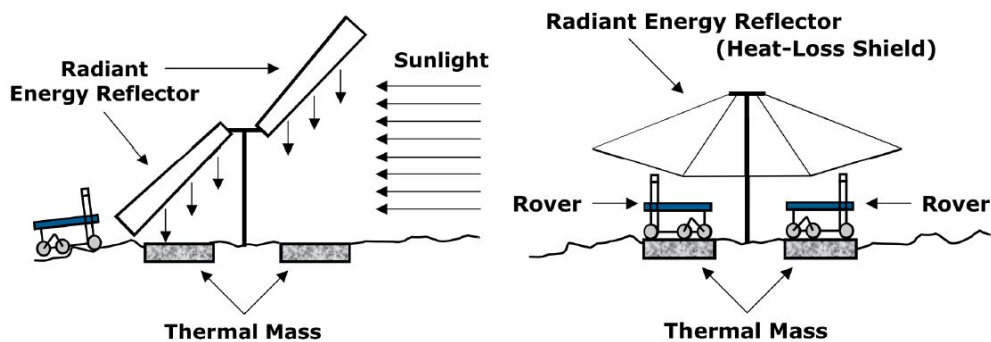
Figure 3.1 Conceptual Figures of Thermal Wadis [9]

Notsu et al. [17] proposed a method for lunar night survival that involves heat exchange with a lunar lander by installing heaters under the lunar surface. This idea

involves maintaining a high regolith temperature using a heater installed under the Moon's surface during the daytime period, when there is enough sunlight and excess power is generated. Subsequently, when the sunlight fades and the Moon's night period begins, the Moon lander receives heat from the regolith, which was maintained at a high temperature by the heater during the Moon's day period. Figure 3.2 shows a conceptual diagram of this proposal. This proposal should aim to develop suitable methods of installing heaters under the Moon's surface.
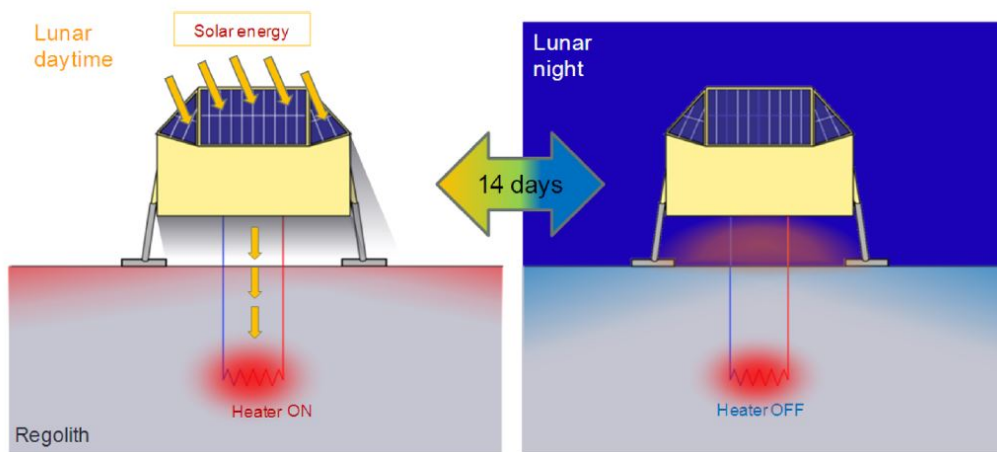
Figure 3.2 Schematic view of using High Heat Storage Capability of Regolith [17]

Okishio et al. [20] proposed a heat exchange device with regolith for night survival. Considering that temperature swings are remarkably small during the daytime and nighttime periods at depths of only 1 m below the surface of the Moon, the device penetrates the surface of the ground below the lunar lander to enable night survival through heat exchange with the regolith. This proposal should identify feasible methods

for penetrating the string through the lunar surface. Figure 3.3 [20] shows the conceptual figure of this idea.
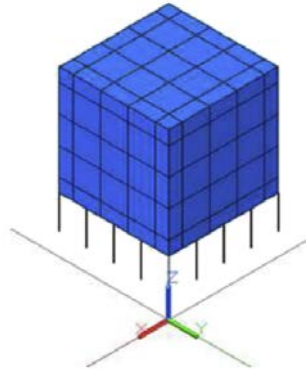
Figure 3.3 Lander Model with String [20]

3.4 A Proposal of MLI Curtain System

Okishio et al. [20] proposed the MLI skirt as an auxiliary means in addition to strings for heat exchange with lunar surface regolith for lunar night survival. The basic concept of this study is similar to the MLI skirt as a shelter for a small rover for lunar night survival. However, unlike the skirt introduced in the study by Shogo Okishio et al. [20], the MLI is configured in a curtain shape to allow small rovers to freely enter and exit the curtain. Figure 3.3 to Figure 3.5 show conceptual configurations of the MLI curtain system for a small rover.
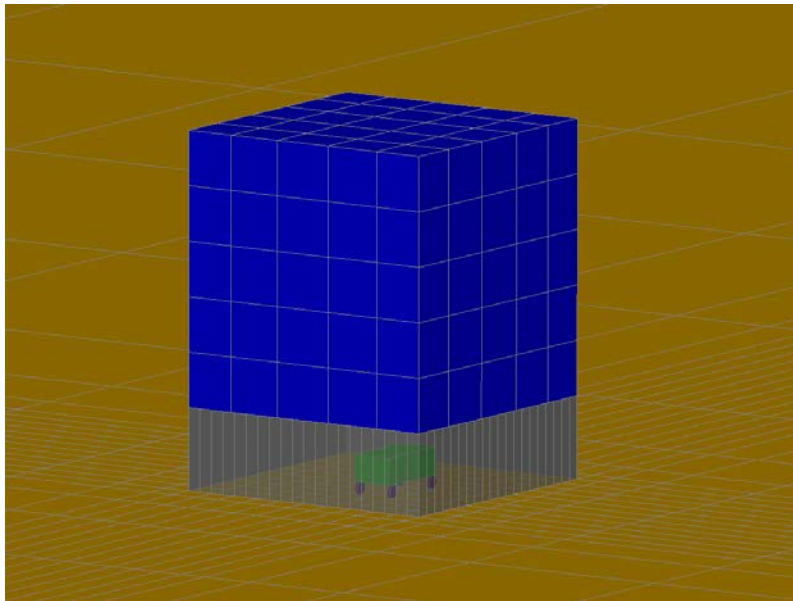
Figure 3.4 A rover in shelter of a lander during lunar nights
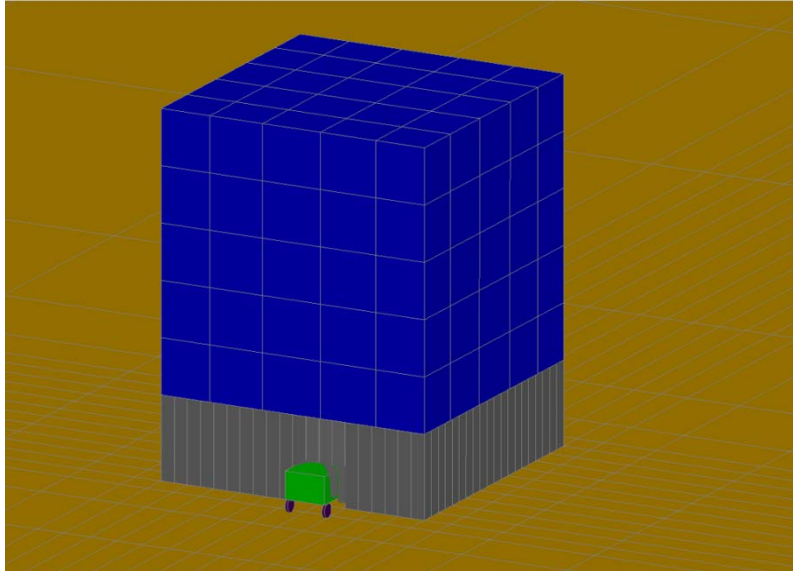
Figure 3.5 A rover moving outside of a lander at lunar dawn
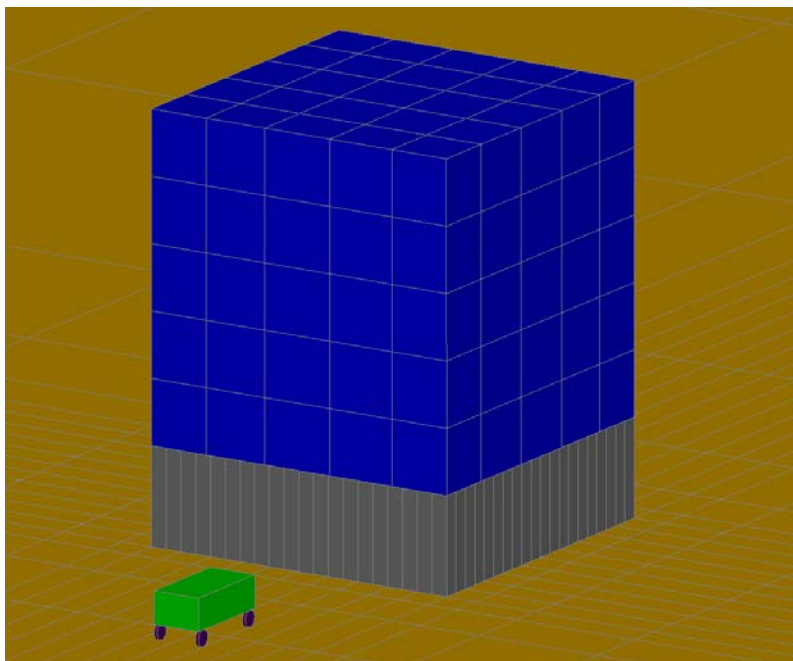
Figure 3.6 A rover in outside of a lander during lunar day

The shape of the MLI curtain proposed in this study is similar to vertical blind curtains used in a typical home. The system has the advantage of allowing the rover to pass through the MLI curtain without assistance from any special opening/closing mechanisms. As shown in Figure 3.3, a rover can survive in a shelter during lunar nights and move out from the shelter through the MLI curtain on its own during the lunar daytime, as shown in Figure 3.4 and Figure 3.5.

In this study, the temperature of the lander during lunar nights can be maintained using RHUs and a lid. Tae-Yong Park et al. [18] introduced a lunar lander thermal model and presented analysis results for lunar night survival. According to their results, the combination of a lid and RHUs was more effective compared to other thermal control devices such as louvers or heat switches. The combination of a lid and RHUs was implemented in the Lunokhod series [7], which were lunar exploration rovers of the former Soviet Union.

From a thermal control perspective, RHUs have the disadvantage of generating heat not only during lunar nights but also during lunar daytime. Although RTGs can produce electrical power even without sunlight, such devices have large volumes, significant weights, and low efficiency. Considering the case of the Galileo probe [21], which employed an RTG that weighed up to 56kg with a capacity of 300W, RHUs are more suitable for lunar night survival compared to RTGs for small landers.

3.5 Cost Effectiveness of MLI Curtain System

As described in Eq. 1.1, the cost of a spacecraft increases significantly with mass. In order for a rover to achieve lunar night survival through thermal wadis [9], as introduced in Figure 3.1, it is necessary to manufacture thermal wadis and construct an energy reflector that acts as a shield. To implement this concept, an additional rover is required to perform the necessary auxiliary tasks, which incurs greater costs than the production cost of the rover that performs the main mission.

As shown in Figure 3.3, the lunar night survival method involving heat exchange with regolith using strings requires spacecraft engineers to consider of the mass of the string itself in spacecraft design. According to a calculation by Okishio et al. [20], in the case of a 1m cubic lander, the desired performance can be obtained by adding approximately 50kg of string, which significantly increases the development cost of the lunar lander-rover system.

Compared to these methods, the MLI curtain system is a highly cost-effective alternative.

Considering the additional missions that a small lunar rover can perform with the MLI curtain system, it may be possible to observe wider areas of the lunar surface based on longer mission durations. In addition, the method allows rovers to acquire lunar surface data that varies over long periods of time. Moreover, with power charging from the lander, a rover's mission can be extended into the lunar night.

Ultimately, spacecraft are designed and constructed for the purpose of performing

and completing space missions. A spacecraft can be considered to be more cost effective if it is capable of performing more missions than other spacecraft of equal production cost. The MLI curtain system, which can increase the mission duration of rovers without requiring additional special equipment, is a potent method that can significantly increase the cost effectiveness of lunar spacecraft.

Chapter 4. Implementation of the MLI Curtain System

4.1 Technical Challenges of the MLI Curtain System

When introducing a new system for spacecraft, the spacecraft design should offer solutions to technical challenges in various subsystems in addition to the thermal control subsystem. The proposal of this thesis cannot be implemented if the MLI curtain system is not feasible with other subsystems. This chapter considers the technical challenges that are expected when implementing the MLI curtain system and presents ideas for solutions.

4.1.1 Deployment Devices of the MLI Curtain

The expected technical challenge of the MLI curtain system in terms of the structure mechanics subsystem is the deployment device of the MLI curtain. As the MLI curtain consists of a material with very weak stiffness compared to the structure of a spacecraft, it is desirable to have the curtain supported by the structure until the spacecraft lands on the lunar surface, after which it is subsequently deployed. As a method of deploying the MLI curtain, it is possible to consider deploying a structure to which the MLI is attached using a mechanism such as motor. In addition, it is possible to consider a method in which the structure holding the MLI curtain is momentarily separated by a device such as non-explosive actuators (NEA) [32] or a pyro device.

Significant difficulties are expected when implementing the MLI curtain deployment method of deploying a structure using mechanisms such as a motor. This is due to the

44

problem that the individual deployment structures are required to hold an excessive quantity of MLI pieces. A realistic means of deploying the MLI curtain is to hold the ends of the curtains with a deployment device at the bottom of the lander, which then deploys the curtains using a release device. A device that holds another device on a spacecraft during launch and then deploys and separates the latter at a certain point after launch is called a Hold Down & Release Mechanism (HDRM).

Among the various HDRMs, a pyro-technique device is a device that cuts and separates connection lines using explosives. Whereas this explosive device is quick and simple to use, it has the disadvantage of significantly impacting the spacecraft [34]. Considering that MLIs are comprised of materials that are easily damaged by physical force, pyro-technique devices are considered as an unsuitable means of deploying MLI curtains.

NEAs (non-explosive actuators), a different type of HDRM, are classified according to methods involved: burn wire mechanisms or shape memory alloys (SMA) [55], depending on the type of material to be implemented. Here, the burn wire mechanism involves the principle of separating bolts and nuts by passing current through wires that hold the nut segments connected with bolts. Figure 4.1[33] illustrates a conceptual diagram explaining the burn wire mechanism.

In Figure 4.1 (a), the nut, which is divided into two pieces, is fixed by a tightening spring and holds the bolt. In Figure 4.1 (b), when a current flows through the fuse wire that fixes the tightening spring, the wire burns and the tightening force of the spring is lost. This loosens the nut, resulting in the bolt being separated from the nut, as shown in

Figure 4.1 (c).
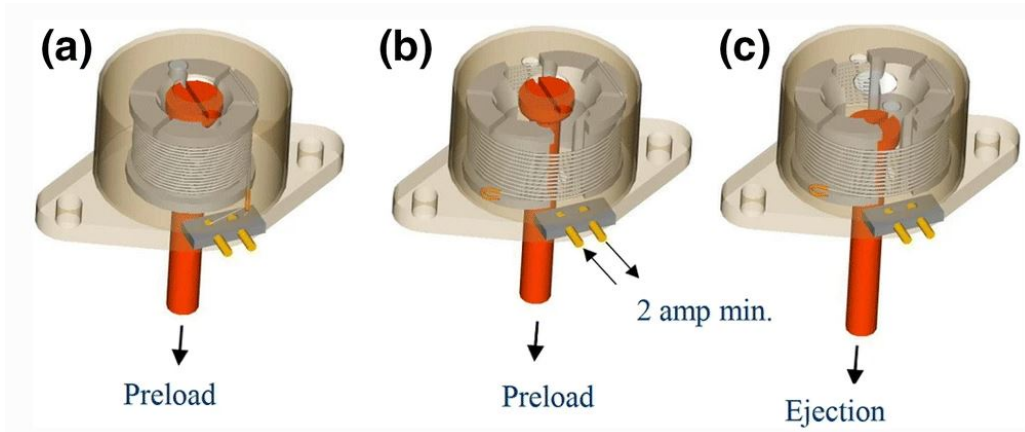
Figure 4.1 Operation principles of a NEA based on the burn wire mechanism [33]

To implement NEAs for the deployment of the MLI curtain, each piece of the MLI curtain should be attached to the lunar lander on one end, whereas the other end is fixed with a bolt. The curtain can be deployed by releasing the bolts through the burn wire mechanism.

4.1.2 Power Charging for Rover

The rover moves into the shelter of the MLI curtain during lunar night periods to be protected from the outside cryogenic environment, which lasts for approximately two weeks. However, considering that this is a long period of time, it is unclear whether the battery installed in the rover can sufficiently last for this period. Therefore, it is necessary for the rover to receive a certain amount of power from the lander, which has a large

capacity battery, while the rover is sheltered inside the MLI curtain.

Due to the rover possessing mobility, a wireless method is required for the lander to supply power to the rover. Wireless power transfer technology has seen significant development in recent years, and has matured enough to be widely used for commercial purposes, even in personal mobile devices. Figure 4.2 [56] shows examples of typical wireless power transfer types and their characteristics.
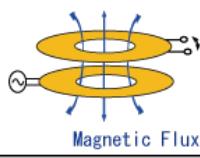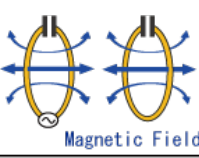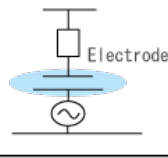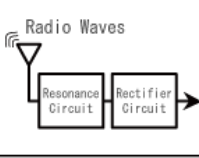
Method	Electromagnetic Induction	Magnetic Resonance	Electric Field Coupling	Radio Receptiong
Configuration	Magnetic Flux	Magnetic Field	Electrode	Radio Waves / Resonance Circuit / Rectifier Circuit
Higher Power Consumption	○	○	◎	△
Efficiency	○ (~90 %)	△ (~60 %)	○ (~90 %)	×
Transmission Distance	× (~several cm)	○ (~several m)	× (~several cm)	○ (~several m)

Figure 4.2 Wireless Charging Methods [56]

The method that uses magnetic fields is simple, inexpensive, and highly efficient when used in close proximities, but has the disadvantage of being sensitive to alignment. On the other hand, the electric field coupling method is highly efficient and relatively less sensitive to alignment, but it can only charge at close proximities. Furthermore, whereas it is possible to transport electrical power over long distances using radio waves, this method suffers from low efficiency. Figure 4.3 [36] describes the categories of wireless power transfer systems that have been developed to date.
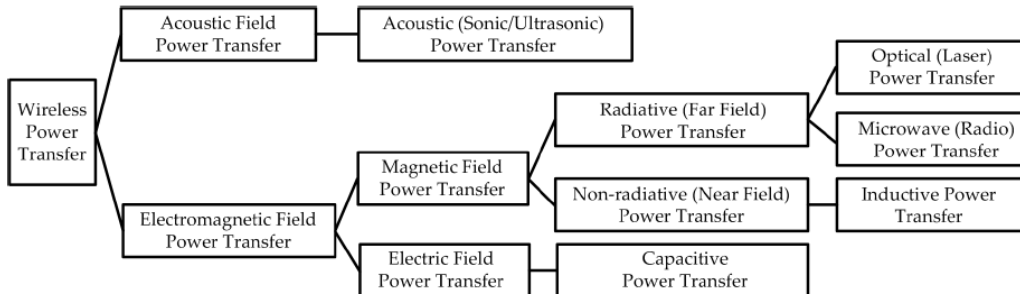
Figure 4.3 Categories of wireless power transfer systems [36]

The electric field coupling method in Figure 4.2 corresponds to the capacitive power transfer (CPT) category in Figure 4.3. Among the high-efficiency charging methods detailed above, a CPT system is deemed to be a suitable choice to charge the rover with the lander for the method proposed in this study. This takes into consideration the unpredictable surface conditions of the landing point on the Moon, which can render perfect alignment difficult. Thus, magnetic field power transfer methods that require perfect alignment are not suitable options.

Figure 4.4 [36] illustrates the general operation concept of a CPT system.
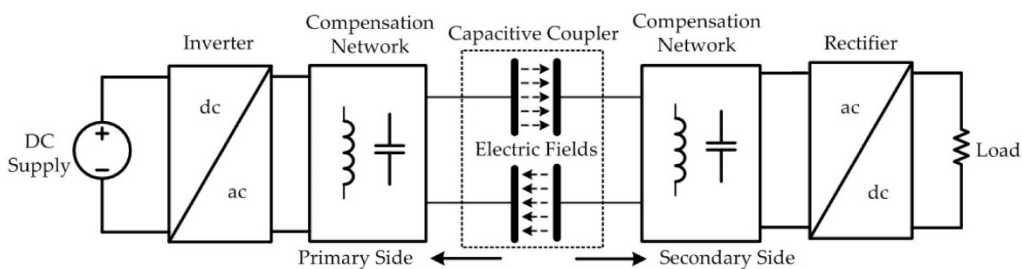
Figure 4.4 Typical structure of a capacitive power transfer (CPT) system [36]

A system that allows the rover to be supplied with power by the lander becomes more important and useful in the case of rovers that are not installed with solar cells, as will be mentioned in Section 4.3. If there are no solar cells on a rover, it must be charged in the shelter of the MLI curtain not only during lunar nights but also during lunar daytime. Considering the significant research on wireless power transfer technology conducted by the private sector and the development of a wide array of related commercial products, it is thought that the rover power charging method proposed in this thesis can be successfully implemented.

4.1.3 RTB (Return to Base) Algorithm

In the method proposed in this thesis, the rover performs missions outside the MLI curtain during the daytime period of the Moon, but returns to the shelter within the MLI curtain when the lunar night begins. If the rover fails to enter the MLI curtain shelter, its power supply from the Sun will be cut off and the rover will inevitably fail due to its inability to overcome the cold conditions of the lunar night. Therefore, the RTB (return-to-base) algorithm that guides the rover back to the MLI curtain shelter is highly important. Moreover, the RTB algorithm is crucial as the rover should be capable of performing RTB operations not only at predetermined times but even when its safe mode is executed.

RTB algorithms are a technology that have yet to be applied in the field of space vehicles, but it is widely implemented in the commercial sector and is a relatively less complex technology. In the case of robot vacuum cleaners that are used in modern homes,

49

CHAPTER 4. Implementation of the MLI Curtain System

not only is RTB technology applied for charging terminals, but further research has been conducted on optimal pathfinding technology [35].

In the case of the MLI curtain system presented in this thesis, RTB algorithms are highly important for rover survival. Fortunately, the technology can easily be implemented by introducing existing technology from the commercial field.

4.2 The Shape of MLI Curtain

In this study, an MLI curtain was used to achieve lunar night survival for a rover. The MLI curtain provides shelter to the rover to prevent radiative heat exchange with the outside environment and to perform heat exchange with the lander. MLI curtains should also allow the rover to pass freely, and possess the ability to completely block external views. This study recommended that the MLI curtain should be designed in the shape of blinds of several pieces. In order to prevent heat loss from gaps between the pieces of the blind shape, the MLI curtain could be designed with two layers and installed in a staggered manner to enhance feasibility. Figure 4.5 shows the configuration of a double layer MLI curtain.
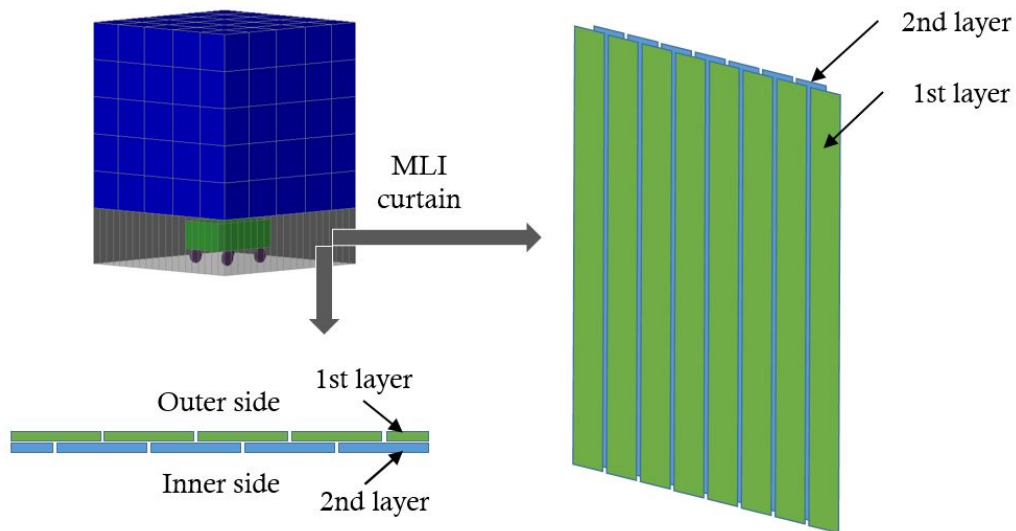
Figure 4.5 Conceptual configuration of a double layer MLI curtain

4.3 Suggestion of the Rover without Solar Cells

In this study, it was assumed that the rover performs missions by charging power through solar panels, as in the case of rovers that were launched in the past. Based on the concept of sheltering the rover within the MLI curtain during lunar nights, removing of the solar panels and SAR (Solar Array Regulator) devices from the rover and, instead, charging energy from the lander, may be considered.

Rovers that convert solar energy into electrical energy are unable to perform missions during lunar nights. Conversely, rovers that perform missions by charging energy from a lander are able to perform lunar night missions, depending on the available capacity of the lander battery. In addition, rovers that are not equipped with solar panels and SAR devices weigh less, making it easier to meet mass requirements. Therefore, by increasing the capacity of the battery by a certain mass, a rover can successfully perform lunar night missions. However, without solar panels on the rover, there exists the restriction of having to return to the lander to charge the rover battery if the remaining energy of the rover battery is insufficient, even during lunar days.

A rover that employs a battery-charging method and performs missions during lunar nights have significant advantages, as it is possible to assign larger mission goals in terms of scientific inquiry. The technology that enables a small rover to recognize the position of the charging device that is equipped in the lander reflects the automatic charging technology of commercialized robot cleaners for home use, which is a technology that can be easily implemented.

Chapter 5. Thermal Modeling

5.1 Governing Equation

Heat transfer encompasses conduction, convection, and radiation. Due to the lack of an atmosphere in outer space, only conductive and radiative heat transfer are considered for thermal analysis of spacecraft. Conductive heat transfer can be expressed with the Fourier's law governing equation shown below.

$$q_{cond} = -k\nabla T \qquad \text{(Eq. 5.1)}$$

Fourier's law refers to the physical phenomenon in which the amount of conductive heat transfer of an object is proportional to the temperature gradient. In Eq. 5.1, q_{cond} is the amount of heat transferred per unit area and unit time, k is thermal conductivity, and ∇T is the temperature gradient. A negative sign in Eq. 5.1 means that heat transfer occurs in the direction from high temperature to low temperature. The one-dimensional conductive heat transfer equation considering a unit area can be expressed as Eq. 5.2.

$$Q_{cond} = -kA\left(\frac{dT}{dx}\right) \qquad \text{(Eq. 5.2)}$$

In Eq. 5.2, the unit of Q_{cond} is W (watt), k is thermal conductivity with the unit W/m/K, and A represents the cross-sectional area with the unit m^2.

The mechanism of radiative heat transfer is understood through the Stefan-Boltzmann law assuming black body radiation, as shown in Eq. 5.3.

53

$$Q_{b,emit} = \sigma T_s^4 \qquad\qquad\qquad \text{(Eq. 5.3)}$$

In Eq. 5.2, q_{emit} is the radiant energy emitted from the surface of a black body per unit area and unit time, T_s is the surface temperature of the black body, and σ is the Stefan-Boltzmann constant with a value of $5.67 \times 10^{-8}\ W/m^2 K^4$.

As described in Section 2.3, real objects are not black bodies but can be simulated as gray bodies with an emissivity (ε) value. The radiation emission of a real object considering the area of the object can be expressed as Eq. 5.4.

$$Q_{g,emit} = \varepsilon \sigma A_s T_s^4 \qquad\qquad\qquad \text{(Eq. 5.4)}$$

In Eq. 5.4, emissivity (ε) is a constant with a value range of $0 < \varepsilon < 1$, and A_s represents the surface area of the object.

Returning to the black body case, the heat transfer $Q_{b,i \to j}$ from the black body face i to the black body face j is given by Eq. 5.5.

$$Q_{b,i \to j} = \begin{pmatrix} Radiation\ leaving \\ the\ entire\ surface\ i \\ that\ strikes\ surface\ j \end{pmatrix} - \begin{pmatrix} Radiation\ leaving \\ the\ entire\ surface\ j \\ that\ strikes\ surface\ i \end{pmatrix}$$

$$= A_i E_{bi} F_{i \to j} - A_j E_{bj} F_{j \to i} \qquad\qquad \text{(Eq. 5.5)}$$

Here, $F_{i \to j}$ is called a view factor and represents the ratio of energy reaching surface

j to the total radiant energy leaving surface i. The view factor is calculated through a complex calculation formula according to the distance between the i-plane and the j-plane, the shape of each object, and the viewing angle. Calculations by hand are not possible unless it involves regular shapes and mutual positions.

The view factor exhibits the reciprocity relation property [3], as described in Eq. 5.6.

$$A_i F_{i \to j} = A_j F_{j \to i} \qquad \text{(Eq. 5.6)}$$

Substituting Eq. 5.6 into Eq. 5.5 gives the following Eq. 5.7.

$$Q_{b,i \to j} = A_i F_{i \to j} (E_{bi} - E_{bj}) = A_i F_{i \to j} \sigma (T_i^4 - T_j^4) \qquad \text{(Eq. 5.7)}$$

The radiative energy transfer of an actual object can be assumed to be similar to a gray body, which has emissivity (ε, $0 < \varepsilon < 1$) values, unlike a black body with absorption and emissivity of 1. In addition, an opaque object has a sum of absorptivity (α, = emissivity) and reflectivity (ρ) of 1, which is described in Eq. 5.8 below.

$$\alpha_i + \rho_i = 1 \qquad \text{(Eq. 5.8)}$$

The radiation emitted from a gray body is given by Eq. 5.4, but the reflection of radiant energy from the outside also occurs. The sum of the two radiant energies becomes the total amount of radiant energy leaving the gray body. In addition, radiant energy that leaves gray body i and reaches gray body j and is again affected by absorptivity, meaning that a portion of the energy is absorbed whereas the remaining energy is reflected.

Therefore, the radiant energy transmitted by gray body i to gray body j is influenced by coefficients, with the emissivity and view factor of the i-plane and j-plane as variables. Assuming B_{ij} is derived with emissivity (ε) and view factor (F_{ij}) as variables, Eq. 5.7 can be arranged as follows.

$$Q_{g,i \rightarrow j} = A_i \sigma B_{ij}(T_i^4 - T_j^4) \qquad \text{(Eq. 5.9)}$$

B_{ij} cannot be hand-calculated except for a simplified sealing system or a shape that follows certain rules. For this reason, several methods have been proposed to obtain B_{ij}. A program such as TRASYS (Thermal Radiation Analyzer System) was used by NASA to calculate B [53], but due to the limited number of nodes, this process took a very long time and had poor accuracy compared to modern programs. Furthermore, efforts were made to obtain B_{ij} with a program using the mesh subdivision method [31], but this also requires a significant amount of time to complete the calculation. In this study, the analysis was performed using a thermal desktop program [5] that calculates B_{ij} using the Monte-Carlo technique.

The thermal capacitance of an object refers to the energy required to raise the unit temperature per unit weight, and the unit is expressed as J/kg/℃ in terms of SI units. Using the definition of thermal capacitance (C_p), the relationship between heat and temperature difference can be expressed as Eq. 5.10.

$$Q = mC_p \frac{dT}{dt} \ (watt) \qquad \text{(Eq. 5.10)}$$

As stated earlier, the thermal equilibrium of a spacecraft without convection is represented by conductive heat transfer and radiative heat transfer. According to Eq. 5.2, Eq. 5.9, and Eq. 5.10, the equation of thermal equilibrium at node i for numerical analysis is expressed as Eq. 5.11 below.

$$\rho V \frac{C_p}{\Delta t}\left(T_i^{n+1} - T_i^n\right) = Q_i + \sum_{j=1}^{n}\left[\frac{kA_{ji}}{L_{ji}}\left(T_j^n - T_i^n\right) + \sigma A_j B_{ji}\left\{(T_j^n)^4 - (T_i^n)^4\right\}\right]$$

(Eq. 5.11)

In Eq. 5.11, ρ is the density of the object, V is the volume of the object, and Q_i is the heat source created at node i. In Eq. 5.11, all variables in the *n*th time step are known values, and only T in the *n*+1th time step is an unknown value. Eq. 5.11 is an equation that is an explicit form of solver. In addition to the explicit form of solver, the Sinda / Fluint [6] program used in this study provides an implicit form of solver, and users are able to select which solver to implement. The solvers exhibit no differences in terms of the accuracy of the analysis results, and the only difference between the two types are in the divergence criteria and convergence time of the numerical solution.

5.2 Thermal Modeling Method of Lunar Surface

Various scientific efforts have been made to simulate the temperature distribution of the lunar surface, as introduced in Section 2.2. Throughout the history of lunar exploration since the 1960s, various models have been developed to model the thermophysical properties of lunar surface materials for the purpose of determining the temperature distribution of the lunar surface, as described in Ref. [27] and [28].

In recent years, the common method of modeling the surface of the Moon involves using a two-layer model, as in the case of Mitchell and de Pater [29] and Ashwin R Vasavada [22]. As demonstrated by the experimental results of the Apollo program [14], [15], the lunar surface layer tends to exhibit thermophysical properties that vary with depth. The two-layer modeling method models the lunar surface by dividing it into a thin layer of fluff and a deeper regolith. The fluff layer is modeled as a very thin, low density, and low thermal conductivity layer, and the regolith layer located below the fluff layer is generally modeled as an object with greater density and thermal conductivity than the fluff layer.

Hager P.B. [10] simulated the density, thermal conductivity, and heat capacity of the regolith as a function based on several previous studies and test results from the Apollo program. The density of regolith is expressed as a function of depth from the ground surface. The thermal conductivity of the fluff layer and the regolith layer are expressed as respective functions of temperature. Lastly, heat capacity is also expressed as a function of temperature to establish a thermal mathematical model of the lunar surface.

Robert J. Christie et al. [11] did not express all thermophysical properties as functions of temperature or surface depth, but instead replaced some properties with constants to facilitate the convenience of performing the analysis without compromising the lunar surface temperature prediction results. Figure 5.1 shows the lunar surface thermal model parameters used by Robert J. Christie et al. [11].
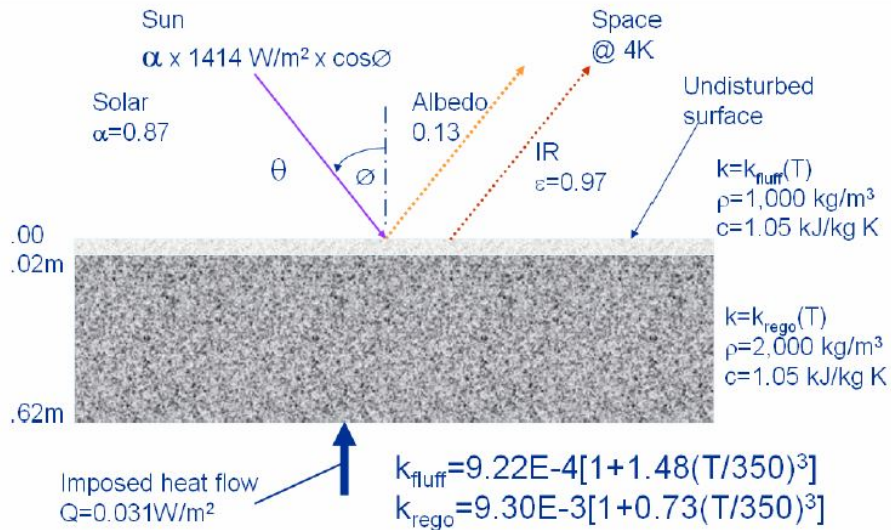
Figure 5.1 Thermal parameters of the lunar surface by Robert J. Christie et al. [11]

T.Y. Kim [30] introduced the Lumped System Model (LSM) to calculate the lunar surface temperature in an analytical manner. Other studies modeled the lunar surface by assuming the heat flux value from the bottom of the lunar surface and the thermal properties of the surface based on existing lunar surface temperature measurement data. Conversely, T.Y. Kim [30] performed lunar surface temperature calculations using the equation for lunar surface energy balance and the data measured by the LRO lunar orbiter.

59

CHAPTER 5. Thermal Modeling

Eq. 5.12 [30] shows the energy equilibrium equation for the lunar surface.

$$C_s \frac{dT_s}{dt} = q_b + q_s - \varepsilon_{IR}\sigma T^4 \tag{Eq. 5.12}$$

In Eq. 5.12, C_s represents the surface heat capacity per unit area, q_b is the conduction heat flux flowing in and out of the surface, q_s is the heat flux from the Sun, ε_{IR} is the emissivity of the Moon's surface, and σ is the Stefan-Boltzmann constant. C_s, q_s, and ε_{IR} were quoted from previous research results, and q_b was derived using Eq. 5.13 [30], which is a function of latitude and longitude. In Eq. 5.13, it is assumed that the subsurface conduction heat flux value (q_b) is proportional to the solar absorption rate at noon, and takes the form of an exponential function as a solution of an ordinary differential equation during lunar nights without incident solar heat.

$$q_b(\psi) = \begin{cases} \alpha_{ss}q_s(\psi_0) - (\alpha_0 + \alpha_{ss})q_s(\psi) & for\ 0 \leq \varPhi < \varPhi_{ss} \\ \alpha_{ss}q_s(\psi_0)exp\left[\ln\left(\frac{\alpha_{sr}}{\alpha_{ss}}\right)\frac{\varPhi-\varPhi_{ss}}{\Delta\varPhi_N}\right] & for\ \varPhi_{ss} \leq \varPhi < \varPhi_{sr} \\ \alpha_{sr}q_s(\psi_0) - (\alpha_0 + \alpha_{sr})q_s(\psi) & for\ \varPhi_{sr} \leq \varPhi < 2\pi \end{cases} \tag{Eq. 5.13}$$

In Eq. 5.13, ψ represents the solar incidence angle and $\varPhi$ represents the longitude. Here, α_{ss} is a constant at sunset, α_0 is a constant at noon, and α_{sr} is a constant at sunrise. When applied as a formula, Eq. 5.14, Eq. 5.15, and Eq. 5.16 [30] are given as

follows.

$$\alpha_0 = \frac{q_s(\psi_0) - \varepsilon_{IR}\sigma T_{s,0}^4}{q_s(\psi_0)} \qquad\qquad \text{(Eq. 5.14)}$$

$$\alpha_{ss} = \frac{c_s(dT_s/dt)_{ss} + \varepsilon_{IR}\sigma T_{s,ss}^4}{q_s(\psi_0)} \qquad\qquad \text{(Eq. 5.15)}$$

$$\alpha_{sr} = \frac{c_s(dT_s/dt)_{sr} + \varepsilon_{IR}\sigma T_{s,sr}^4}{q_s(\psi_0)} \qquad\qquad \text{(Eq. 5.16)}$$

To obtain solutions for the above equations, the measurement data of LRO are used: the result of Eq. 5.13 can be derived using the temperature and slope values obtained by LRO. Kim applied the best curve fitting [30] to recalculate the relevant coefficients, and was able to calculate the surface temperature of the Moon based on Eq. 5.12.

In the results shown in Figure 5.2, the calculation results of Kim are not continuous around sunrise and sunset and do not match the actual measurement data. In Kim's LSM equation (Eq. 5.12), the left-hand term is set as zero during the daytime with solar radiation, but it has a non-zero value at the sunrise and sunset points, the boundary line in which solar radiation disappears. Therefore, the resulting discontinuity occurs due to the thermal inertia of the left-hand term. All in all, Kim's study [30] is meaningful in that the surface temperature of the Moon was obtained by introducing an analytical method.
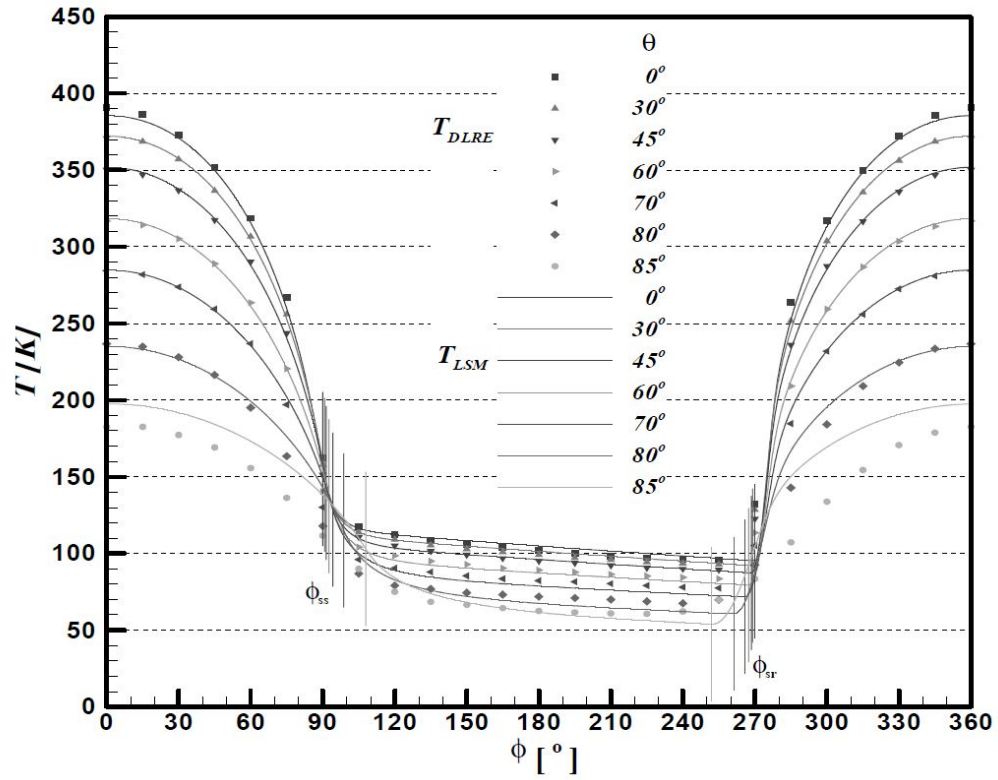
Figure 5.2 Lunar surface temperature calculation results vs LRO measurements [30]

5.3 Thermal Modeling of Lunar Regolith and Verification

Among the studies involving the thermal modeling of lunar regolith and the prediction of lunar surface temperatures by Ashwin R Vasavada[22], Hager, PB[10], T.Y. Kim [30] and Robert J. Christie[11], this study used the thermal modeling method proposed by Robert J. Christie[11]. Of the various thermal modeling variables used by Robert J. Christie[11], only Moon albedo was quoted by Ashwin R. Vasavada's study[23] based on LRO(Lunar Reconnaissance Orbiter) measurement results. The main variables used for lunar regolith thermal modeling are shown in Table 5.1.

Table 5.1 Thermal model variables for lunar surface modeling

Modeling variables	Value
Moon surface IR emissivity	0.97
Moon Albedo[23]	$A(\theta) = 0.08 + 0.045(\theta/45)^3 + 0.14(\theta/90)^8$
Density of fluff (kg/m^3)	1000
Conductivity of fluff (W/m/K)	9.22E-4[x1+1.48(T/350)^3]
Density of regolith (kg/m^3)	2000
Conductivity of regolith (W/m/K)	9.30E-3[x1+0.73(T/350)^3]
Specific heat of fluff and regolith (J/kg/K)	1050
Imposed heat flow (W/m^2)	0.031
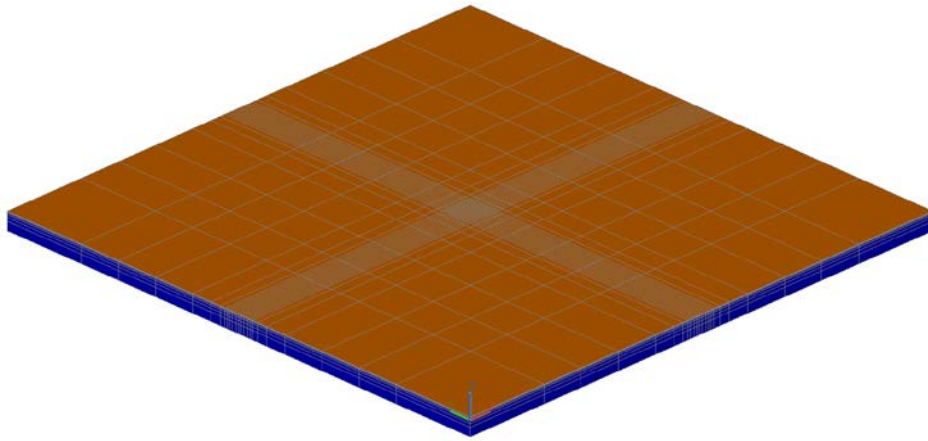
Figure 5.3 Thermal model of lunar regolith

'Fluff' in Table 5.1 is a term referring to a surface layer up to a depth of 0.02 m from the surface of the Moon, and 'regolith' is a deeper layer. In other sections of this thesis, 'regolith' will refer to a combination of fluff and regolith. The thickness of lunar regolith was modeled as 0.6 m. Figure 5.3 shows the result of modeling lunar regolith. The modeling and analysis of the lunar regolith were conducted using Thermal Desktop[5] and Sinda-Fluint[6]. The central part of the lunar regolith model was further subdivided as the lunar lander and the rover are located at the corresponding location. This ensures that the radiative heat exchange between the lunar surface and the lunar lander and the rover further improves the reliability of the analysis.

The regolith model simulates the temperature change of the regolith due to its rotation as it moves along the Moon's rotation cycle. Figure 5.4 shows that the regolith model is based on the equator of the Moon and moves according to the Moon's rotation cycle during one lunar day.
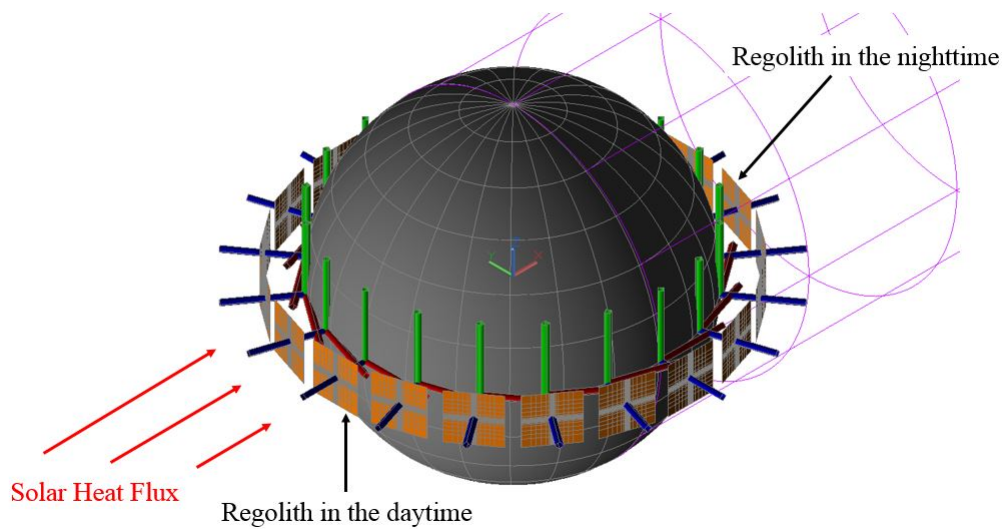
Figure 5.4 Locations of regolith model during 1 lunar day

In order to verify the lunar regolith thermal model, we used the LRO lunar surface temperature measurement data from Williams, J.P., Paige[24] as a reference. The reference data values and analysis results are shown in Figure 5.5 to Figure 5.8. In Figure 5.5 to Figure 5.8, the x-axis is the angle from the Sun to the Moon, and the y-axis is the temperature of the lunar surface with units in absolute temperature (K).
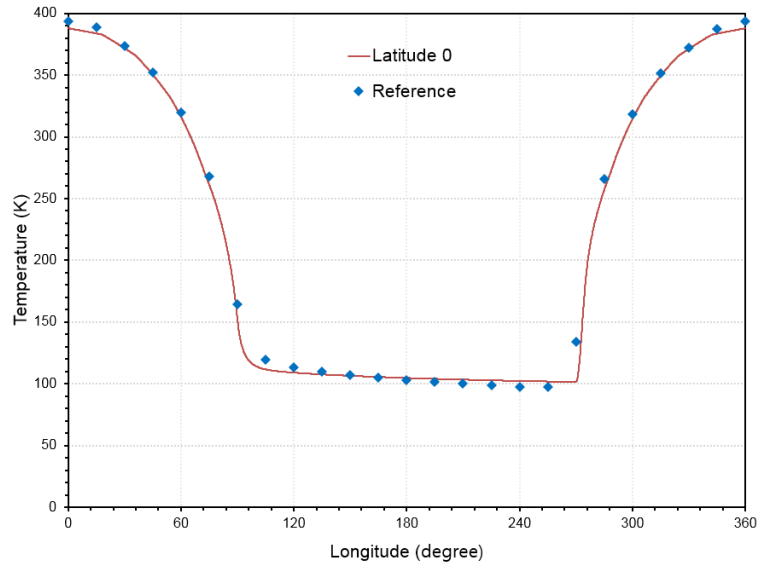
Figure 5.5 Calculated temperatures of the lunar surface at Latitude 0°
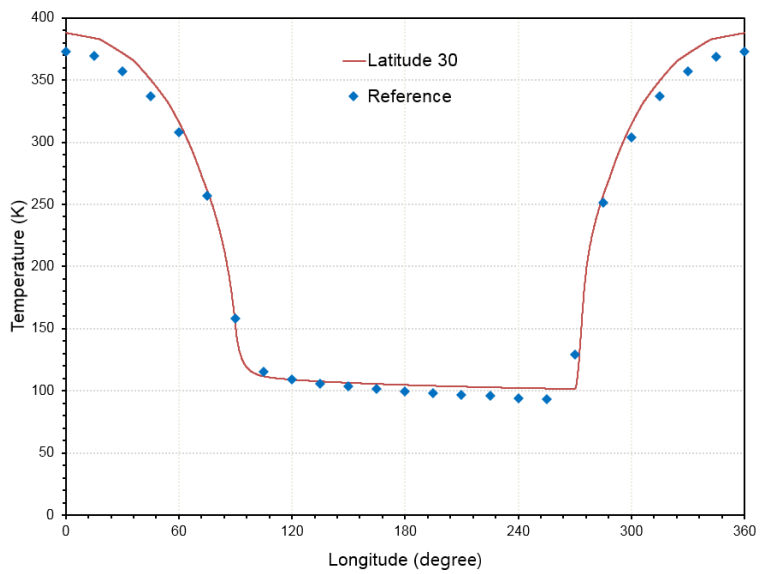
Figure 5.6 Calculated temperatures of the lunar surface at Latitude 30°
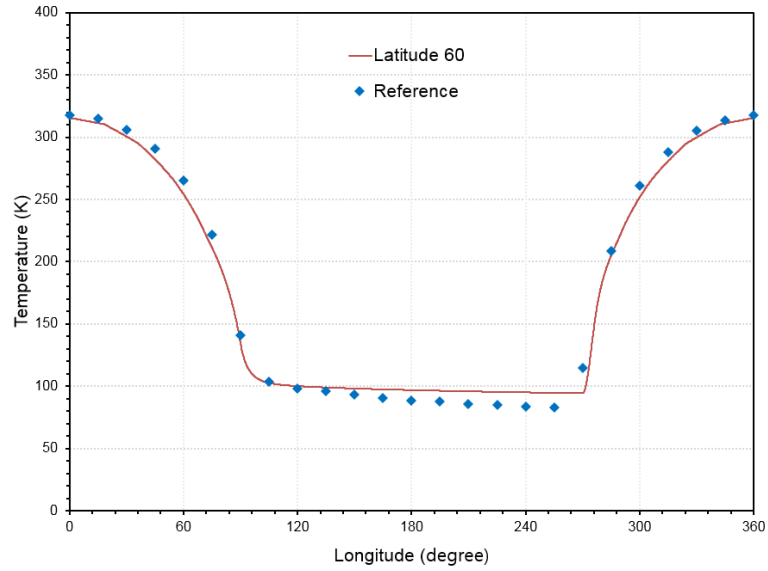
Figure 5.7 Calculated temperatures of the lunar surface at Latitude 60˚
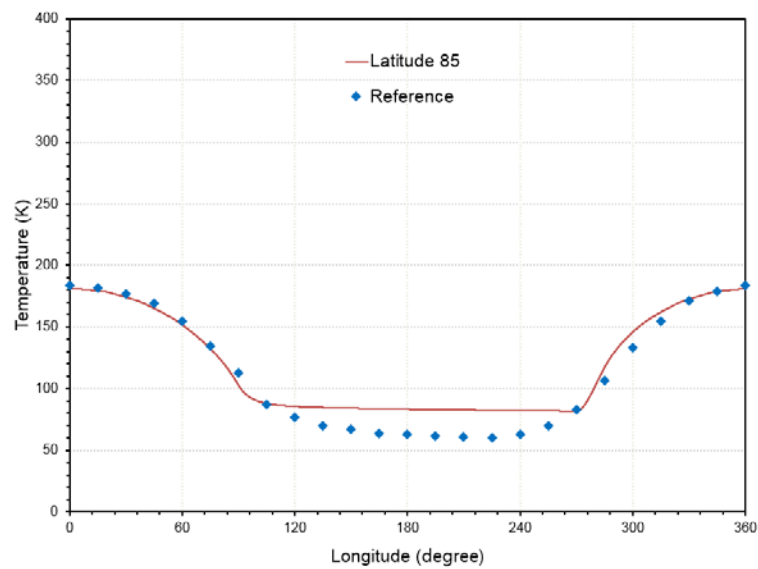
Figure 5.8 Calculated temperatures of the lunar surface at Latitude 85˚

CHAPTER 5. Thermal Modeling

Figure 5.5 to Figure 5.8 show that the analysis results of the lunar surface temperature were similar to the LRO measurement data for the latitude 0º and latitude 30º cases. On the other hand, in the case of latitude 60º and latitude 85º, there were slight deviations on the cold side of the Moon as the modeling variables presented in the study by Robert J. Christie[11] were values derived by approximation for all positions in lunar surface modeling. Considering that the landing sites of lunar landers launched to date were mostly between latitude 0º and latitude ±40º[42], in addition to the fact that the landing position of the lunar lander and the rover in this study is also latitude 0º, Figure 5.5 to Figure 5.8 show that the proposed regolith modeling possesses sufficient accuracy to be utilized here. In this study, the landing position of the lunar lander and the rover was set to latitude 0° as the position of latitude 0° is the worst from a thermal perspective due to having the largest temperature difference between day and night on the lunar surface. This follows the basic rules of thermal design/analysis to confirm the survivability of landers and rovers even under the worst thermal conditions [2]. In addition, analysis was performed for latitude 30 ° and latitude 60 ° to compare the results.

5.4 Thermal Modeling of the Lunar Lander and the Rover

With the purpose of this study being to review a lunar night survival method for a small lunar rover, the thermal model of the lunar lander and the rover was made as simple as possible.

Table 5.2 Assumed specifications of the lunar lander and the rover

Lunar Lander	
Dry Mass	300 kg
Size (L·W·H)	1m x 1m x 1m
Specific Heat	900 kg/J/K
Conductivity	20 W/m/K
Heat Dissipation (Day / Night)	120W / 10W
Operating Temperature Range	-20℃ ~50℃
Rover	
Mass	25 kg
Size (L·W·H)	0.4m x 0.25m x 0.15m
Specific Heat	900 kg/J/K
Heat Dissipation (Day / Night)	15W / 0.5W
Operating Temperature Range	-15℃ ~45℃

Table 5.2 shows the specifications and temperature requirements of the small lunar

lander and the rover that were assumed in this study.

The thermal model of the lunar lander was designed as a cubic shape consisting of 125 nodes with the width, length, and height being five nodes long. The thermal conductivity of the lander model was assumed as 20 W/m/K, which is 1/8 of the thermal conductivity of general aluminum, instead of the internal radiation heat exchange in the empty space inside the lunar lander. Table 5.2 shows that the heat dissipation of the lunar lander was 120 W during the day and 10 W during the night as the heat dissipation of the lunar lander was assumed as shown in Table 5.3.

Table 5.3 Assumed power consumption of the lunar lander

Unit	Day (Mission profile)	Night (Sleep mode)
Main Computer	40 W	5 W
Power Converter & Distributer	40 W	3 W
Communication Transponder	20 W	1 W
Battery	0 W	1 W
Location & Attitude Sensors	5 W	0 W
Lander Payloads	15 W	0 W
Total	120 W	10 W

As the average power consumption during a lunar night was assumed as 10 W in Table

5.3, the battery capacity of the lunar lander should be at least 3600 Wh (= 15 days x 24 hours / day x 10 W) for lunar night survival. In this case, assuming the typical specific energy of a battery as 145 Wh/kg[12], the minimum mass of the required battery is calculated as 24.8 kg. With the mass of the lunar lander assumed in this study being 300kg, the mass of the battery is approximately 8% of the total dry mass. Considering that the mass ratio of the battery in the Apollo lunar landing mission was approximately 1%[43], the battery mass ratio of this study is not a small value.

As the assumed mass of the battery of this study was already high, it was difficult to increase the capacity of the battery to consume heater power during lunar nights. Therefore, it was concluded that the supply of the heat source for lunar night survival should solely depend on the RHU. If heater power is consumed for lunar night survival, an incremental increase in battery capacity of 360 Wh is required for the consumption of 1 W of heater power, which results in a 2.5 kg mass increase per watt. Such effects make it increasingly difficult to meet lander mass requirements.

Figure 5.9 and Figure 5.10 show the thermal model of the lunar lander and the rover of this study. Thermal Desktop[5] and Sinda-Fluint[6] were used for thermal modeling and analysis of the lunar lander and the rover as well as the land regolith.

As illustrated in Figure 5.9, the lunar lander was modeled as a 1 m x 1 m x 1 m cube, and the lunar surface was modeled as a 20 m x 20 m square as in Shogo Okishio's[20] study. In order to improve the accuracy of the analysis, the node size of the lunar surface in the vicinity of the lunar lander was smaller compared to nodes located further away from the lander.
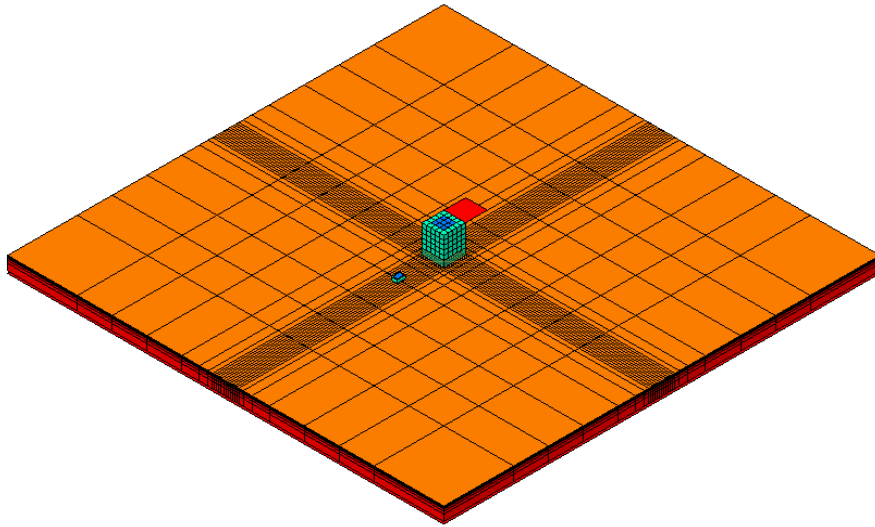
Figure 5.9 Thermal model of the regolith, the lander, and the rover
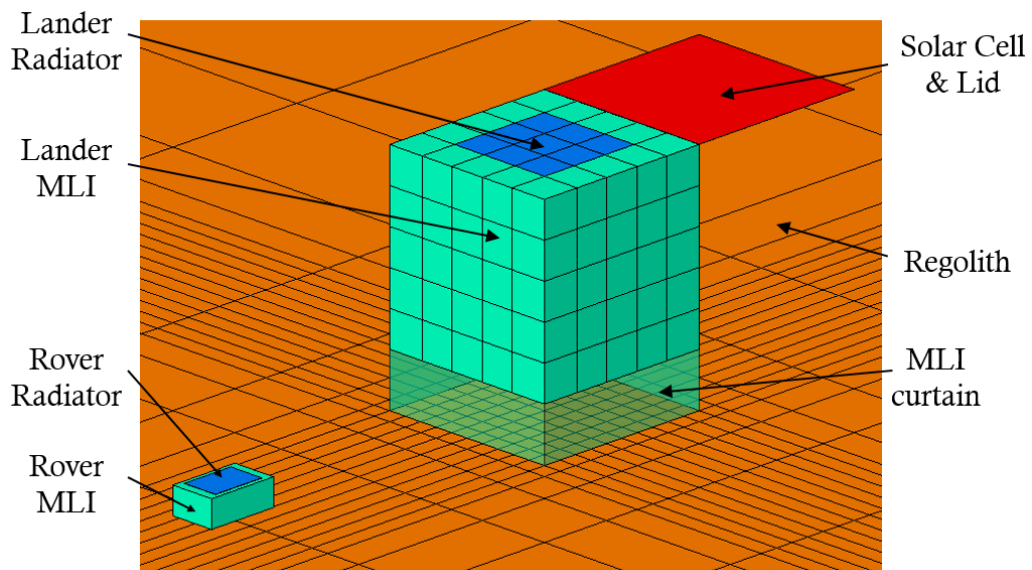
Figure 5.10 Thermal model of the lander and the rover

As shown in Figure 5.10, the lunar lander was designed as a cubic model with a total

of 125 nodes. In order to efficiently radiate heat without interfering with the surrounding surface temperature, a radiator was installed in the direction of deep space.

As shown in Table 5.2, the rover was modeled as a single node that was 40 cm x 25 cm x 15 cm in size with a mass of 25 kg. The power consumption of the rover was assumed as 15 W during lunar day missions and 0.5 W standby power during lunar nights. The standby power of 0.5 W while the rover hibernates inside the MLI curtain during lunar nights means that an additional 1.25 kg of battery mass is required in a similar manner to the situation described in the previous paragraph. As such, it could be concluded that it is important to minimize the standby power of the rover in order to meet the mass requirements of the rover. If meeting the mass requirements of the rover proves challenging, the rover could be charged by the lander during lunar nights, which is an idea further described in section 4.1.

In this study, the model of the MLI uses the CR-model (conduction-radiation model) introduced by C.K. Krishnaprakas[25], which is given by the following Eq. 5.17.

$$Q \; (\text{W/cm}^2) = h'(T_h - T_c) + \varepsilon'_{eff}\,\sigma\,(T_h^4 - T_C^4) \qquad\qquad (\text{Eq. 5.17})$$

In Eq. 5.17, *Q* represents the heat flow rate through the MLI. The MLI specification is assumed to be 10 single spacer layers, the value of *h'* is 7.92E-07 (W/cm^2·K), the value of ε'_{eff} is 3.27E-03, and σ is the Stefan-Boltzmann constant. The values of T_h and T_c in Eq. 5.17 represent the temperatures at both sides of the MLI.

In this study, the radiator optical properties of the lander and the rover were 0.06 for solar

absorption and 0.83 for infrared emissivity, as with the example of the UV reflective-coated OSR (Optical Solar Reflector) of Qioptiq[44]. The bottom surface coating of the lunar lander was designed with black paint to enhance heat exchange with the rover to enhance lunar night survival.

Chapter 6. Thermal Analysis

6.1 Thermal Design Requirements of the Lander and Rover

In order to develop the thermal design of a space vehicle, the thermal design requirements must be determined in advance. The primary purpose of a thermal design is to maintain the temperature of all parts of the spacecraft within acceptable temperature ranges during all missions. Some general examples of detailed thermal design requirements for spacecraft are as follows.

- The specifications of the hardware to be used for thermal control should be space-grade

- A redundancy plan should be in place for single fault error

- The design should consume minimal power during the spacecraft's safe mode

- An override function for heater on/off temperature should be in place

- The design should meet EMI / EMC requirements

- Thermal analysis should be performed under the worst thermal environmental conditions

- Appropriate margins should be considered for thermal analysis

The requirements in terms of the allowable temperature ranges for thermal analysis of the lander and rover are shown in Table 5.2. Among the thermal design requirements listed above, the thermal analysis described in this chapter was performed by applying allowable temperature requirements and worst-case thermal analysis conditions, as these are applicable to the field of thermal analysis.

75

6.2 Thermal Analysis Case

In this study, the lunar exploration rover performs its missions outside the lunar lander during the lunar daytime, and moves back into the lunar lander MLI curtain during the lunar nighttime to survive, as described in the previous section. In addition, the lunar lander covers the radiator with a lid, which is a panel equipped with solar cells during lunar nights, similar to Lunokhod[7]. During lunar nights, the lander solely uses RHUs as a heat source instead of an electrical heater. Figure 6.1 shows that the rover performs its missions outside the lunar lander, during the lunar daytime. In addition, the solar panel of the lander is deployed.
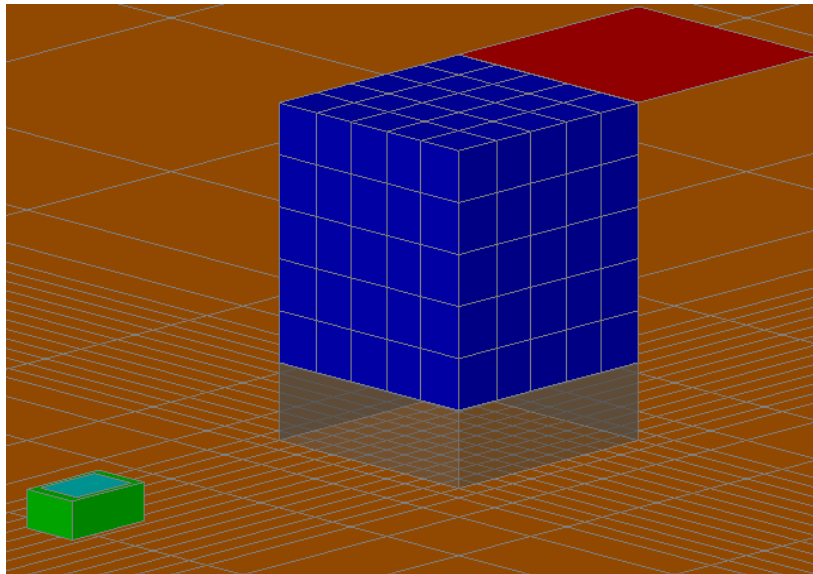
Figure 6.1 Mission configuration of a lunar lander and a rover during a lunar day

Figure 6.2 shows that the rover moves into the MLI curtain of the lunar lander, and the solar panel that acts as a lid covers the radiator to prevent heat loss. As it is required for the solar panel, which acts as a lid, to cover the radiator and perform heat shielding during lunar nights, the design should adopt the application of the MLI to the rear end of the solar panel. The heat dissipation of the lander and the rover for one lunar day is shown in Table 5.2.
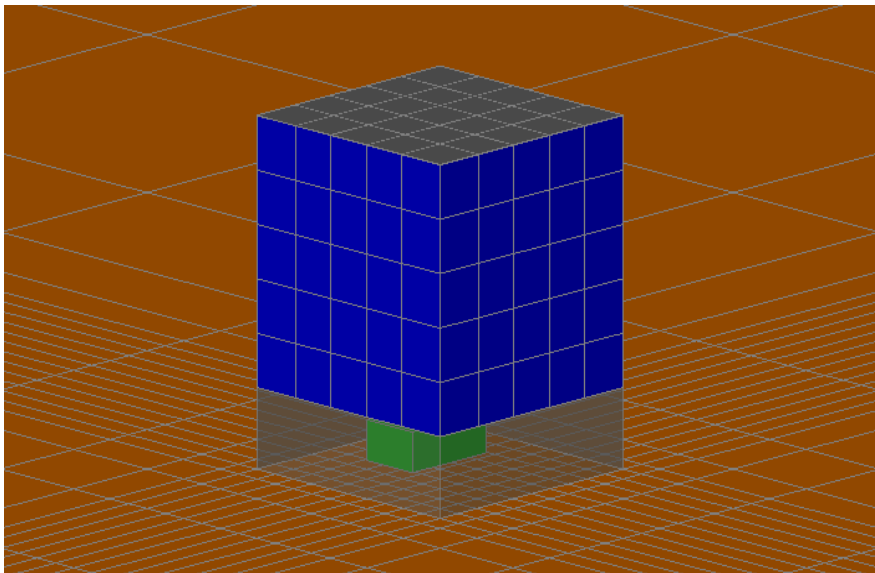
Figure 6.2 Mission configuration of a lunar lander and a rover during a lunar night

The landing position of the lunar lander was set as the latitude 0° position of the Moon, where the temperature variation of the lunar surface is the most extreme. The solar heat flux was assumed as $1366 \, \text{W} / \text{m}^2$. In Figure 6.3, the positions of the lander and the rover at sunrise, noon, sunset, and midnight during a lunar day are shown through a concept

diagram.
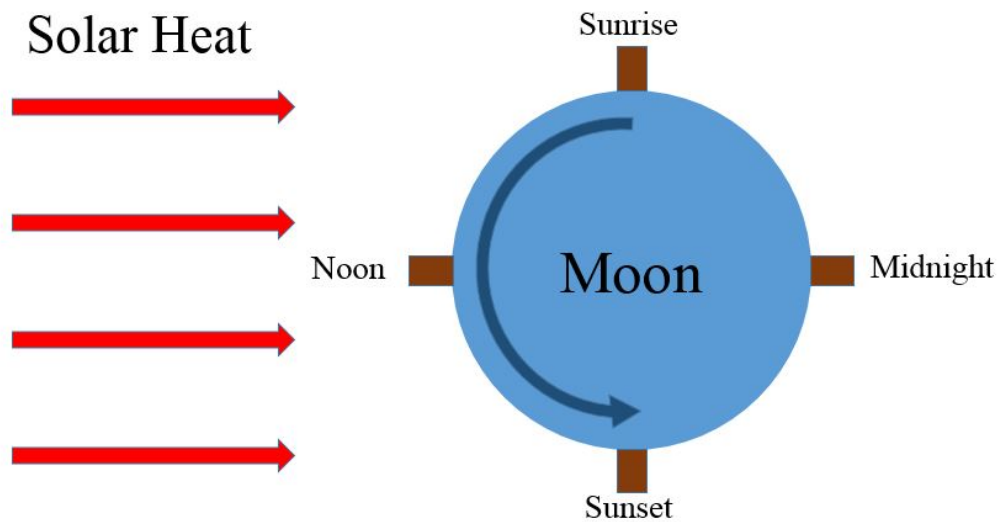
Figure 6.3 Location of lunar lander during 1 lunar day

As stated above, thermal analysis should be performed under the worst-case conditions. As stated in Section 5.3, the most extreme case for thermal analysis among the Moon's mission points occurs at latitude 0°, where the temperature difference between day and night is greatest. Therefore, in this study, the thermal analysis of the lander and rover was based on the position at latitude 0°. The cases of latitude 30° and latitude 60° were also analyzed to observe the temperature changes of the lander and rover. Figure 6.4, Figure 6.5, and Figure 6.6 show the thermal analysis cases at latitude 0°, latitude 30°, and latitude 60°, respectively.
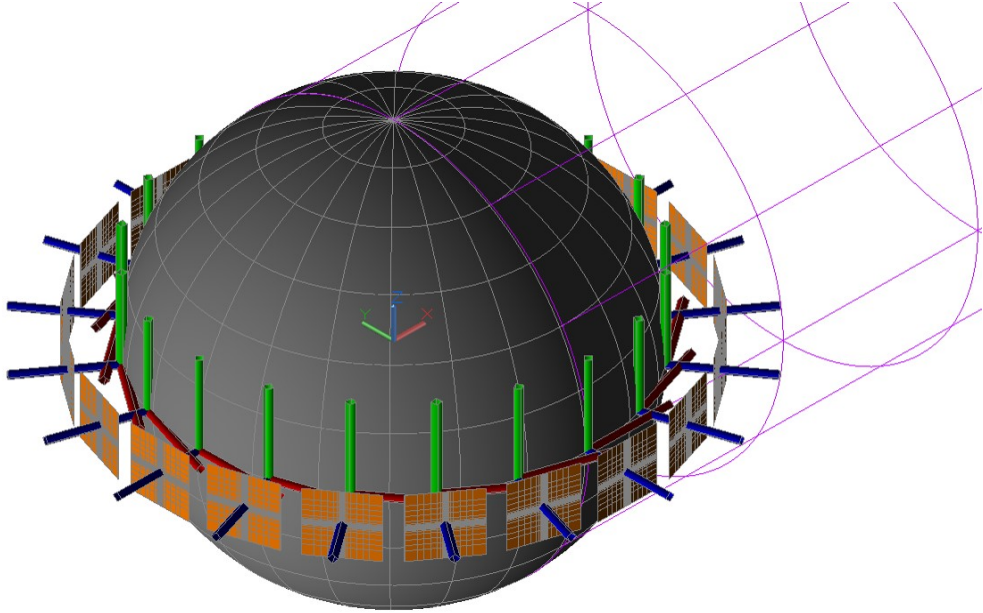
Figure 6.4 Thermal mathematical model results for the latitude 0° case
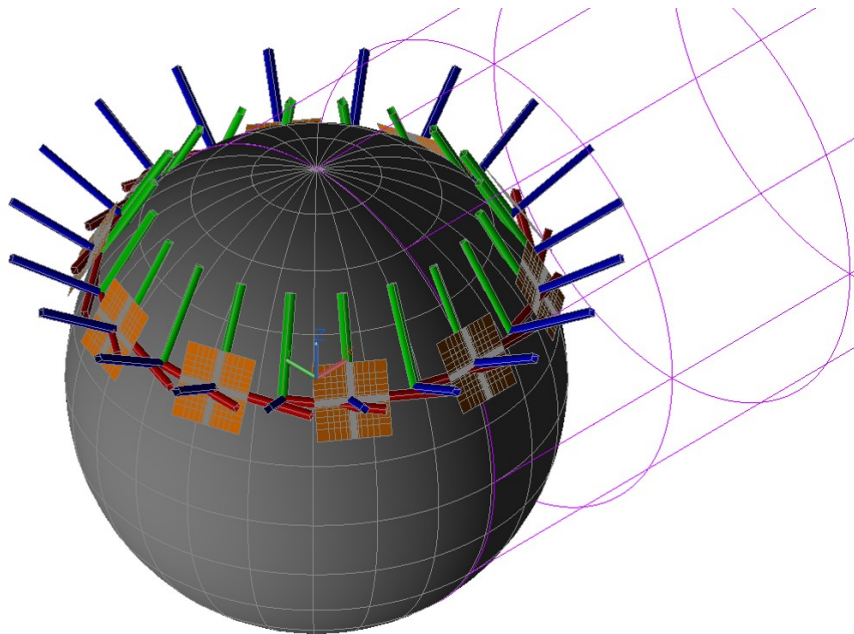
Figure 6.5 Thermal mathematical model results for the latitude 30° case
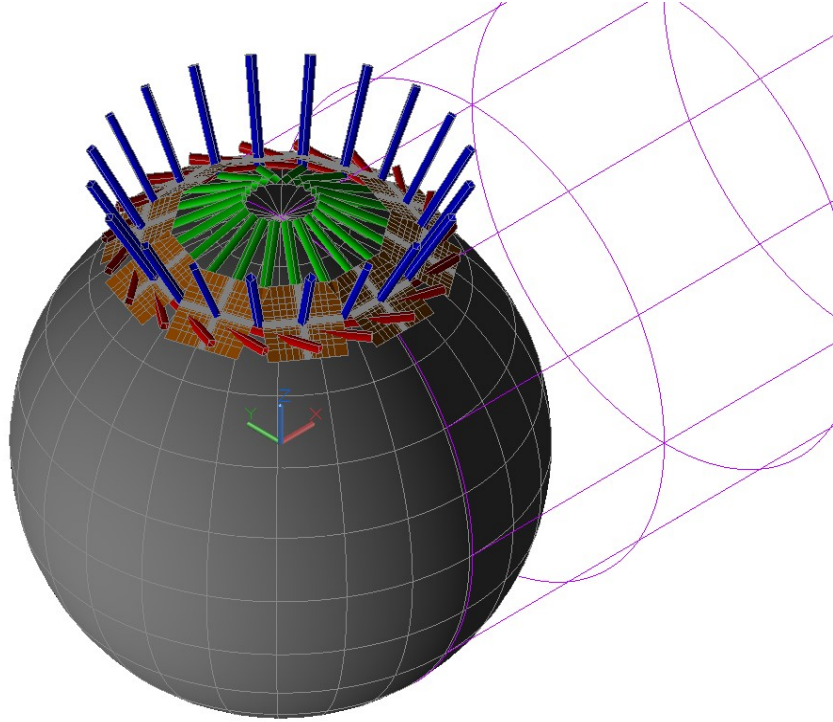
Figure 6.6 Thermal mathematical model results for the latitude 60° case

6.3 Analysis Result of the Radiator Area and a Number of RHU

In order for a small lunar lander to survive in the cryogenic environment of lunar nights, it is efficient to supply heat through RHUs. From a thermal control perspective, RHUs have the disadvantage of continually dissipating heat during lunar days in addition to lunar nights. Therefore, the lunar lander should radiate the heat generated by the RHUs in addition to the heat of the lunar lander itself, and the heat dissipation area should be designed accordingly.

The procedure of designing the radiator area and the capacity of the RHU of a lunar lander is as follows. First, the radiator area of the lunar lander should be designed so that the temperature of the lunar lander does not exceed the maximum acceptance temperature during lunar days under the thermal environment described in Table 5.2. If the lunar lander has no RHU, the temperature of the lunar lander may fall below the minimum acceptance temperature during lunar nights. The design should calculate the proper number of RHUs that prevents the temperature of the lunar lander from falling below the minimum acceptance temperature. Due to the additional RHU heat, the lander temperature rises to higher temperatures during lunar days. Hence, a larger radiator area is required, which should be recalculated. This iterative process is a flow that proceeds with Radiators and Dissipation as variables in the thermal design process of Figure 2.1.

As the lid covers the radiator area during lunar nights, the decrease in temperature due to the greater radiator area is negligible. This completes the design of the radiator area and the RHU. An excessive number of RHUs will increase the risk related to cost and

mass while a too small number of RHUs will increase the risk related to thermal control requirements. Therefore, it is crucial to calculate the appropriate number of RHUs.

In this study, the lunar rover does not equip RHUs. The lunar rover moves into a shelter surrounded by an MLI curtain between the lunar lander and the lunar surface during lunar nights. The radiator of the lunar rover should be designed to ensure that the maximum temperature of the rover does not exceed the maximum acceptance temperature during lunar days.

The RHUs were evenly distributed inside the lunar lander, and heat load of the RHUs evenly distributed 20 watts on the 125 lander model nodes. Assuming that a single RHU weighs 40 grams and possesses a heat load of 0.9 watts[48], the lunar lander requires 22 RHUs with a total mass of 0.88 kg that can supply approximately 20 W of heat.

Table 6.1 shows the radiator area and the RHU capacity of the lunar lander and the rover derived from the aforementioned process.

Table 6.1 Thermal design result of the lunar lander and the rover

Design Category	Value
Radiator Area of the Lander	3600 cm^2
Radiator Area of the Rover	640 cm^2
Heat capacity of the RHUs in the Lander	20 Watt
Required RHUs in the Lander	22 ea.

6.4 Temperature Trends of the Lunar Lander and the Rover

Figure 6.7 to Figure 6.10 show calculated temperature contours of the lunar lander and the rover at latitude 0° and the four locations defined in Figure 6.3. The temperature contours of the lunar lander and the rover shown in Figure 6.7 to Figure 6.10 present the temperatures of the structures, excluding the MLI.

The solar panel was deployed after sunrise (Figure 6.7) and stowed before sunset (Figure 6.9). The lunar rover moved outside the lunar lander after sunrise and returned inside the MLI curtain before sunset.
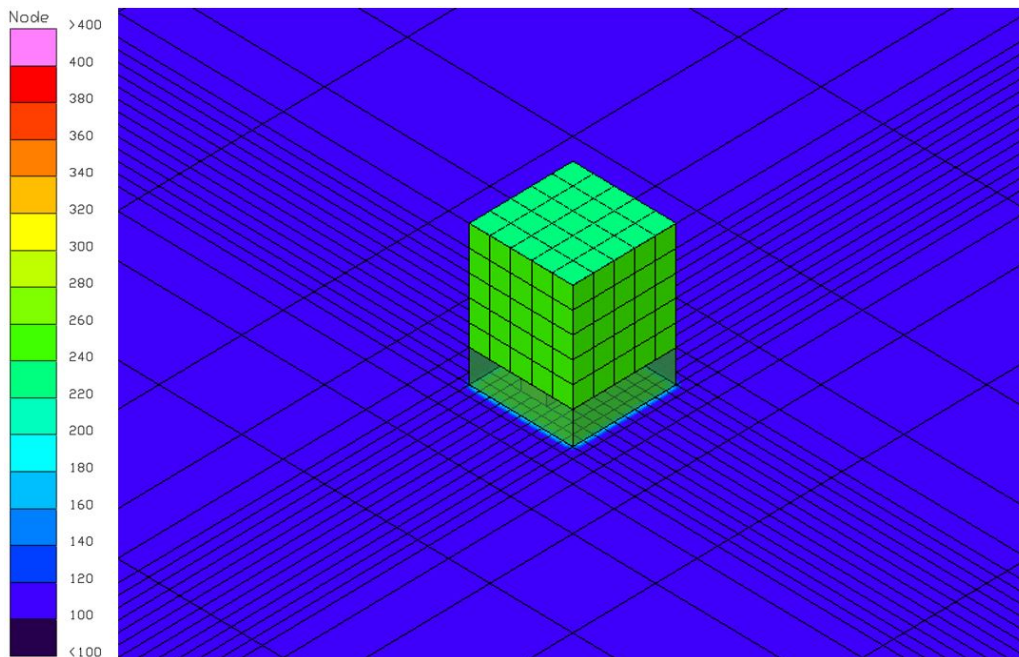
Figure 6.7 Temperature contours of the lunar lander and the rover at sunrise
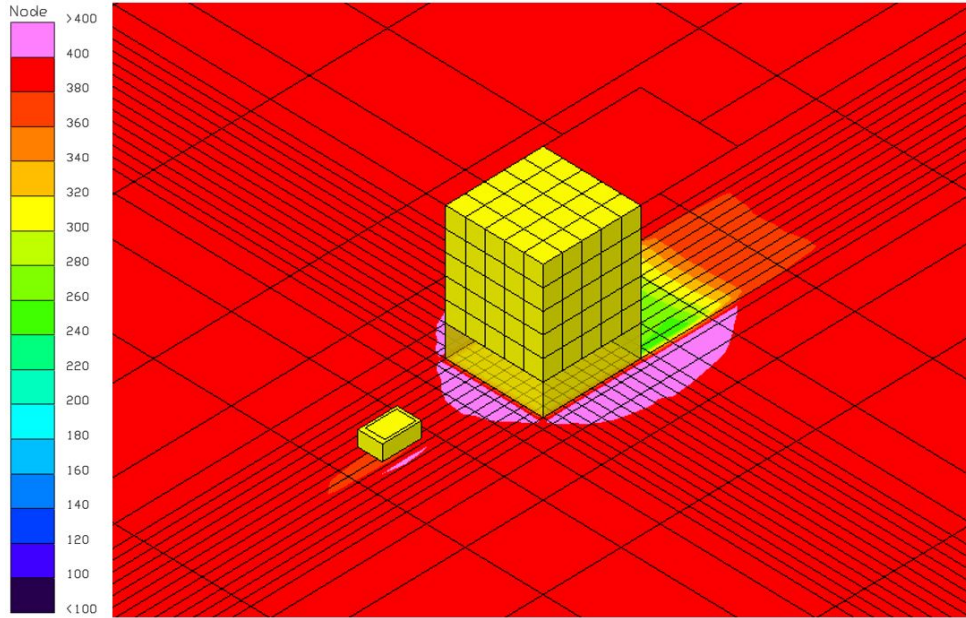
Figure 6.8 Temperature contours of the lunar lander and the rover at noon
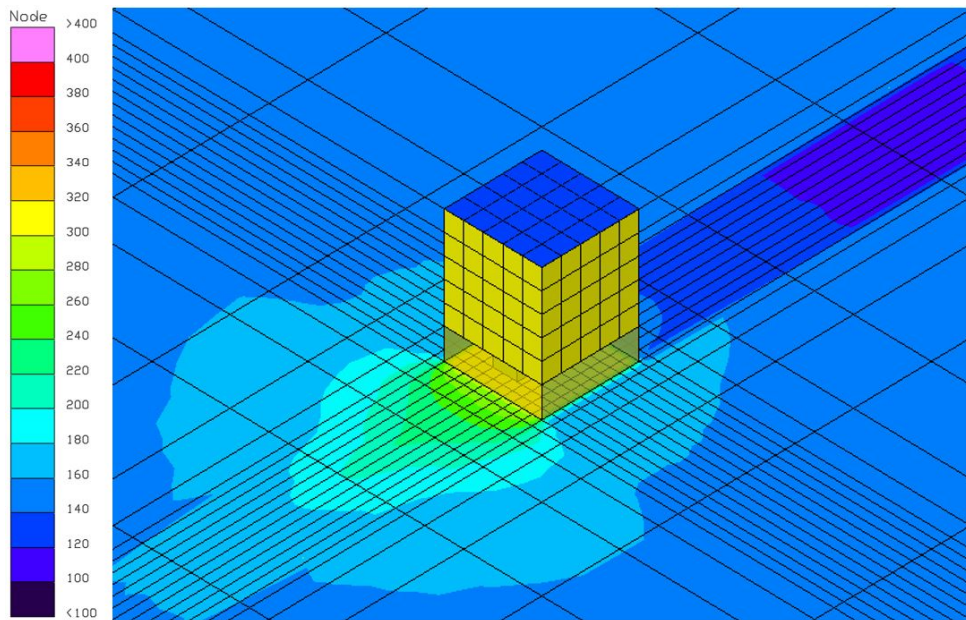
Figure 6.9 Temperature contours of the lunar lander and the rover at sunset
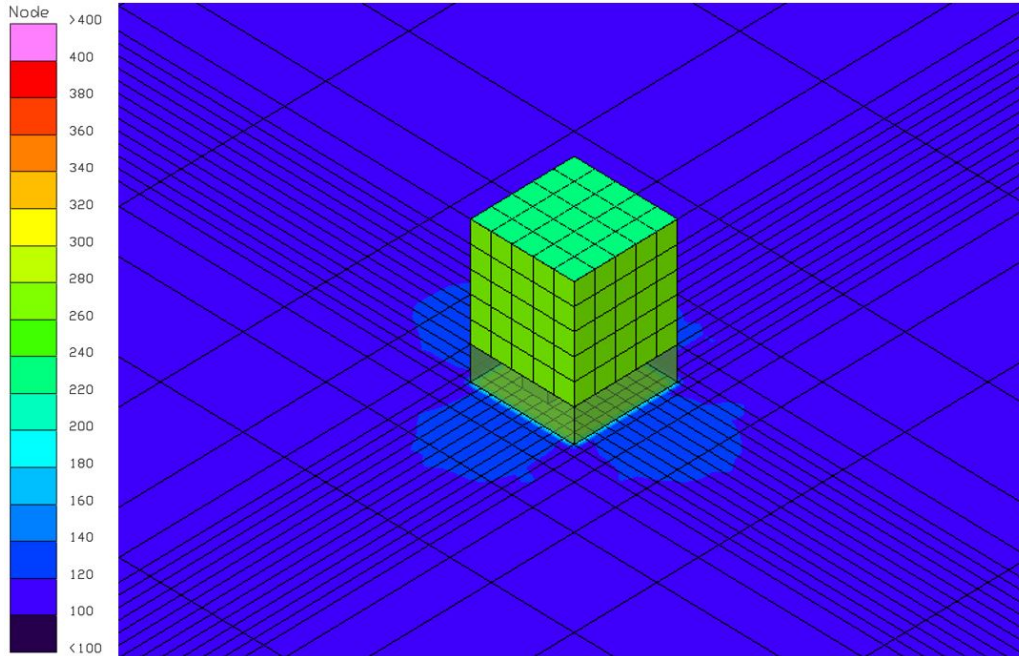
Figure 6.10 Temperature contours of the lunar lander and the rover at midnight

Among Figures from Figure 6.7 to 6.10, the temperature of lunar lander is lowest at sunrise (Figure 6.7) and highest at noon (Figure 6.8). However, the lander reaches a maximum temperature between noon and sunset during a lunar day, as shown in Figure 6.11.

The configuration of the deployed solar panel and the rover performing missions can be seen at the noon location in Figure 6.8. In addition, the temperature of the lunar regolith that was shadowed by the solar panel was observed to be lower than the temperature of the surrounding area due to the blocking of sunlight by the solar panel. At noon, the temperature of the regolith in the vicinity of the lunar lander was observed to be slightly higher than the temperature of the regolith further away from the lander.

85

This is due to sunlight being reflected from the MLI of the lunar lander, resulting in greater incident solar heat at the regolith near the lander compared to regolith further away from the lander. At sunset in Figure 6.9, the temperature at the shadow of the lander is lower than the temperature of surrounding regolith, and the temperature of the regolith at the front end of the lander, which receives incident solar heat reflected by the lander, is higher compared to the surrounding regolith. The solar panel, which also acts as the lid of the lander radiator, receives little sunlight at sunset, which results in a substantially low temperature at sunset. When the solar panel (lid) covers the radiator of the lander, it begins to exchange heat with the lander. As a result, the temperature of the solar panel (lid) was confirmed to be higher at midnight compared to sunset. At midnight, the temperature of the regolith in the vicinity of the lander was observed to be slightly higher compared to the temperature of the surrounding regolith due to radiation heat exchange with the lander. The temperature of the regolith near the lander was observed to be lower at sunrise compared to midnight.

Figure 6.11 shows the temperature trend of the lunar lander during a lunar day. In Figure 6.11, the x-axis represents time, and the point at which the x value is zero indicates sunrise. The point at which the x-value is 354.4 hours indicates sunset, at which the temperature abruptly drops due to the change in the heat dissipation of the lunar lander from 120 watts to 10 watts. Figure 6.12 shows the diagram of the lunar lander thermal model and the description of the variables introduced in Figure 6.11.
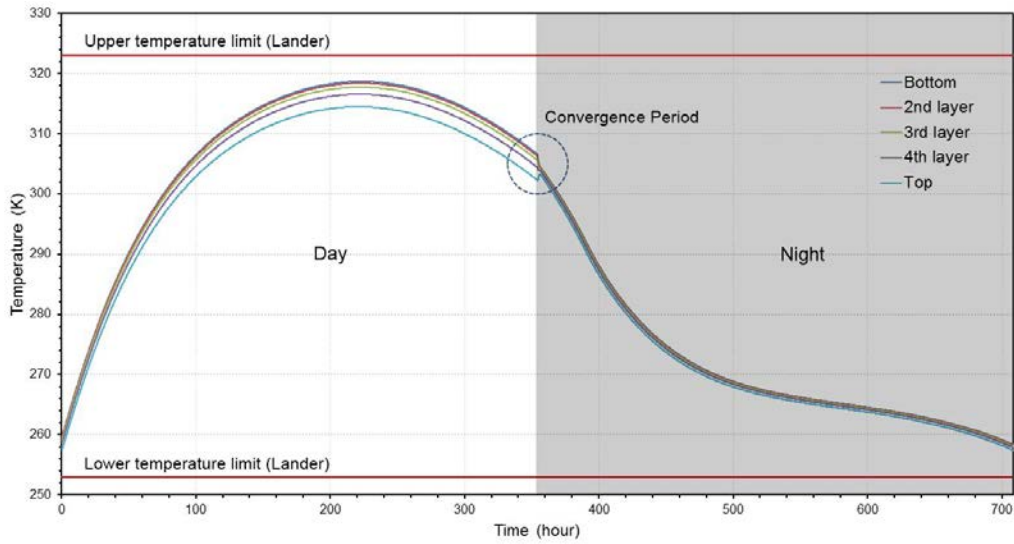
Figure 6.11 Temperature trend of the lunar lander during a lunar day
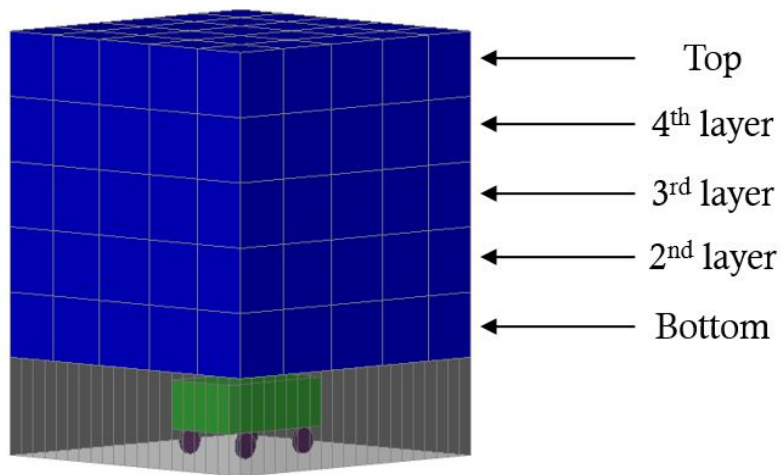
Figure 6.12 Diagram of the lunar lander thermal model

87

CHAPTER 6. Thermal Analysis

Figure 6.11 shows the temperature change at the center of the lander model, divided into five layers in the height direction, for a lunar day. The maximum temperature of the lander occurs at the bottom layer with a temperature of approximately 319 K, which does not exceed the maximum temperature requirement of 50℃ (323 K) specified in Table 5.2. The minimum temperature of the lander occurs at the top layer and is approximately 257 K. This also satisfies the minimum temperature requirement of -20℃ (253 K) in Table 5.2. Therefore, results confirm that the temperature of the lander during a lunar day meets the acceptance temperature requirements in Table 5.2.

When the lander enters lunar nighttime, the lid covers the radiator of the lander, and the heat loss is limited to a minimum. From this point, heat exchange takes place inside the lander for a certain period of time, and the temperature gradient decreases between the lander nodes. This period was termed the 'convergence period', during which the temperatures of the lander nodes converge. The temperature trend during this period is shown in Figure 6.13. As shown in Figure 6.13, the temperature at the bottom of the lander, which possessed a relatively high temperature value, rapidly decreases due to the decrease in the heat dissipation value of the lander. However, the top of the lander, which possesses a relatively low temperature, is temporarily warmed by the heat inflow from inside the lander. Once convergence is achieved over a period, the temperature of the entire lander decreases during the night.
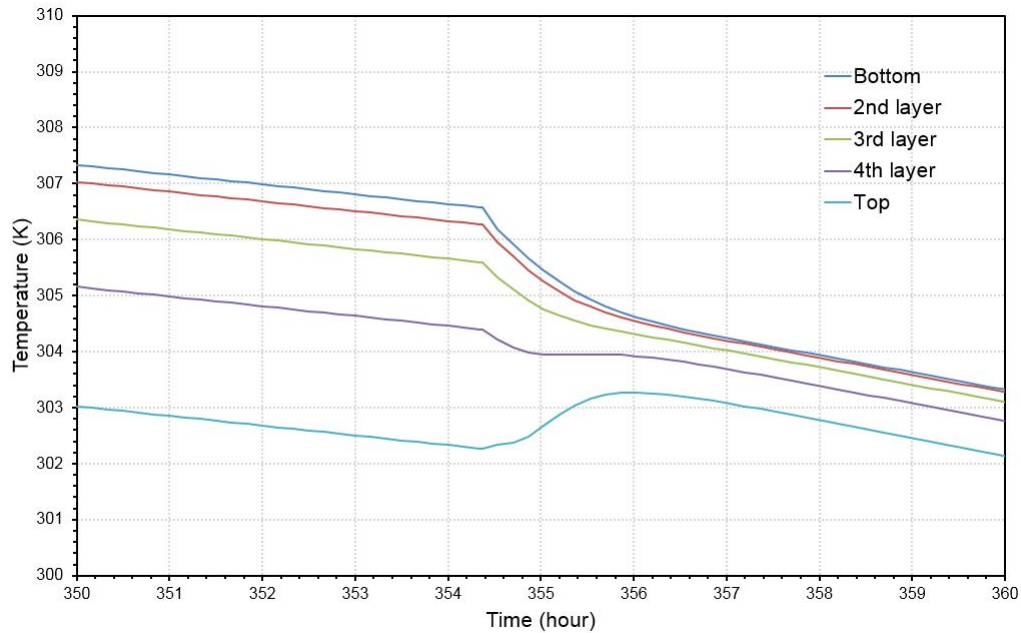
Figure 6.13 Temperature trend of the lunar lander during the convergence period

The highest temperature of the lunar regolith occurs at noon, whereas the highest temperature of the lander occurs between noon and sunset. This is caused by the fact that, although the solar heat input is greatest at noon, the temperature of the lander is further increased past noon as the solar heat input is greater than heat rejection for a certain period. The time at which the temperature of the lander reaches a peak varies depending on the thermal capacity of the lander and the environmental heat exchange situation in the lander.

Figure 6.14 shows the average temperatures of the lunar lander and the rover for a lunar day. In the case of actual rovers that perform lunar missions, a rover does not begin missions precisely at sunrise as it will need to receive solar power and produce electricity

89

to perform its mission. However, in this study, a rover mission is assumed to take place outside the lander from sunrise to sunset to analyze the temperature behavior of the rover under the worst conditions.
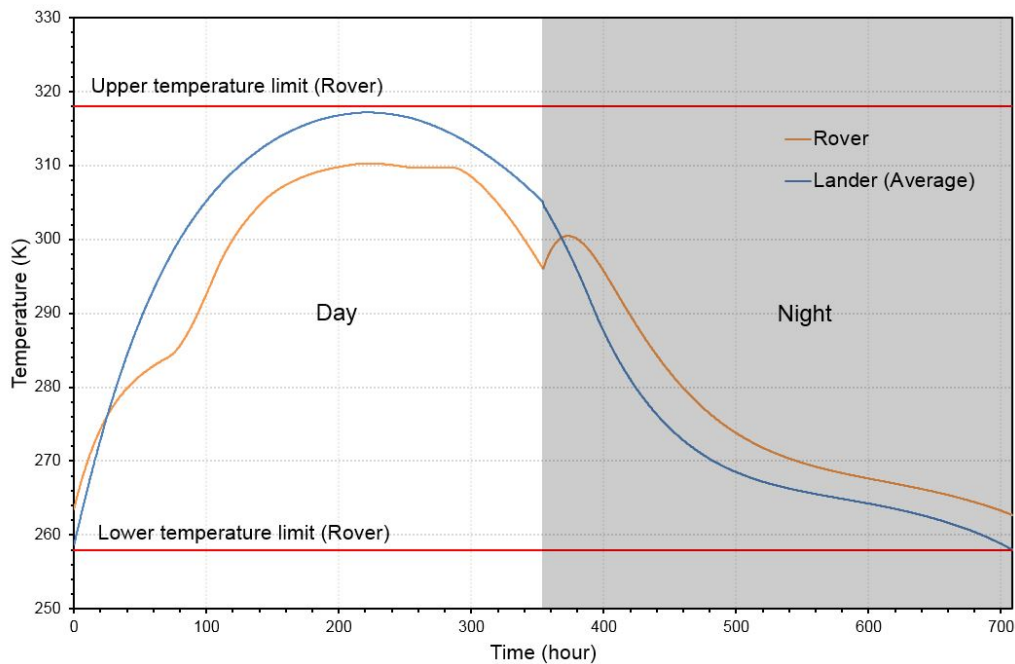
Figure 6.14 Average temperatures of the lunar lander and the rover during 1 lunar day

Figure 6.14 shows that the temperature trend of the rover undergoes several inflections, unlike the temperature trend of the lander. This is due to the small thermal mass of the rover and the various temperature profiles influenced by environmental elements such as sunlight reflected from the lander. Similar to the lander, the rover reaches its highest temperature between noon and sunset due to the continuous input of solar heat even past noon until the rover reaches thermal equilibrium. Due to the relatively small thermal mass of the rover and the fact that the rover is affected by the temperature of the lander

90

(which has a relatively large thermal mass), the temperature of the rover retains a flat shape for a certain period after reaching a peak temperature. This is in contrast to the case of the lander, where the temperature decreases immediately after highest temperature. The temperature trend of the rover is affected by the relative position between the rover and the lander, and the shape of the graph in Figure 6.14 changes according to the changes in the relative position between the rover and the lander.

In Figure 6.14, as the rover moves through the MLI curtain into the shelter for lunar nights, the temperature of the rover rises for a certain period through heat exchange with the bottom of the lander, followed by a steady decrease in temperature as the lander temperature decreases. The temperature of the rover is maintained at a level slightly higher than the lander temperature during lunar nights due to heat from 0.5 W of standby power without heat exchange with the environment outside the lander. As a result, the maximum temperature of the rover is approximately 310 K, which is below 45 °C (318 K), and the minimum temperature is approximately 263 K, which is higher than -15 °C (258 K). Therefore, the temperature of the rover during a lunar day meets the acceptance temperature requirement described in Table 5.2.

In this study, the rover was able to satisfy the acceptance temperature requirement during lunar nights by simply moving into a sheltered location within the MLI curtain of the lander without mounting thermal control devices such as a lid or RHUs. The results confirm that, with assistance from an MLI curtain in the lunar lander, a small rover is able to carry out long-term missions for periods longer than a month, similar to large-sized rovers.

91

In Figure 6.15, the analysis results of the latitude 30° case are compared with the results of the latitude 0° case.
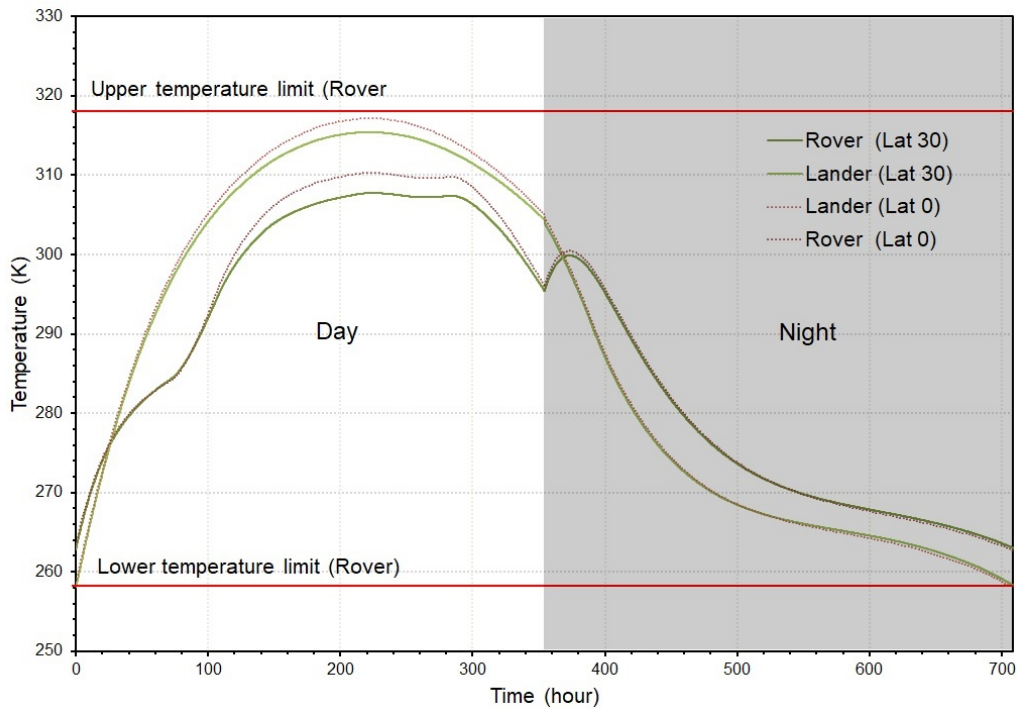
Figure 6.15 Temperature trends of the lander and rover at latitude 0° and latitude 30°

As shown in the graph, the maximum temperatures of the lander and rover are lower at latitude 30° compared to latitude 0°, whereas the minimum temperatures are similar in both cases. This is due to the latitude 0° point corresponding to the worst thermal case, and it is clear that it is easier to meet the thermal requirements of a lander and rover when the missions are performed at latitude 30°.

In Figure 6.16, the analysis results of the latitude 60° case are compared with the results of the latitude 0° case.
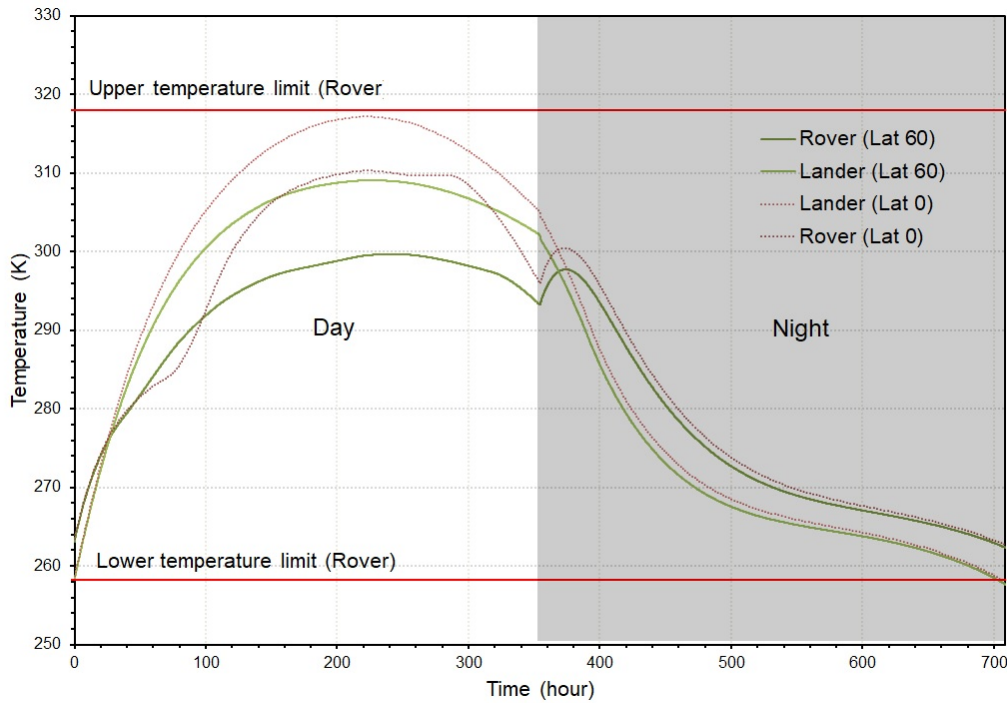
Figure 6.16 Temperature trends of the lander and rover at latitude 0° and latitude 60°

The graph shows that the maximum temperatures of the lander and rover are lower at latitude 60° compared to latitude 0° in addition to latitude 30°. This is due to the lower angle of solar incidence on the surface at latitude 60° compared to latitude 0° or latitude 30°, as shown in Figure 6.6. Therefore, it is easier to satisfy the thermal requirements of a lander and rover if the mission area is located at latitude 60° compared to the other two cases.

6.5 Analysis of the Influence of the RHUs and Lid

In order to examine the efficiency of the lid and RHUs of the lander, the temperature results of the lander without the lid and RHUs were compared with the thermal analysis results of the lander described in the previous section, as shown in Figure 6.17.
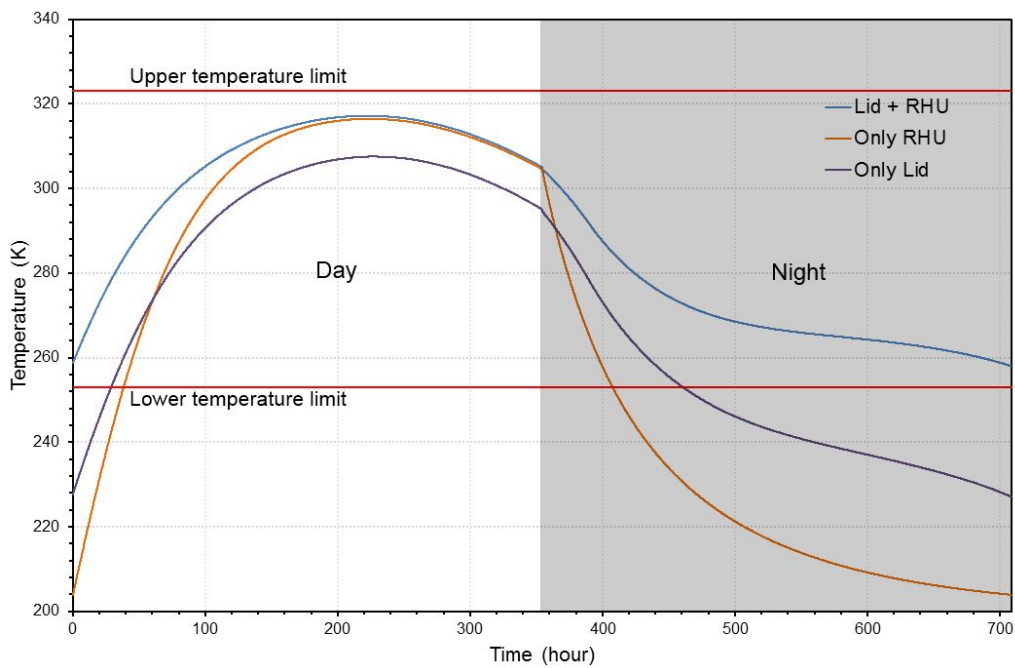
Figure 6.17 Case study on the efficiency of the lid and RHUs

The important focal point of Figure 6.17 is the difference between the maximum and minimum temperatures during a lunar day. If the difference between the maximum and minimum temperatures is small, it is possible to satisfy acceptance temperature requirements even if the temperature results exceed the maximum or minimum acceptance temperatures by shifting the analysis temperature by adjusting the radiator

area. In Figure 6.17, the difference between the maximum and minimum temperatures of the lander is approximately 59 K, according to the analysis of the design results in Table 5.1. The difference is approximately 80 K without the RHUs, and approximately 113 K without the lid. Considering that the temperature difference of the acceptance temperature requirements is 70 K (-20 ℃ ~ 50 ℃), it is difficult to achieve the acceptance temperature requirement without the RHUs and the lid even with adjustments in radiator area.

In the absence of a lid, the temperature drops rapidly after entering the lunar night, resulting in a larger difference between the maximum and minimum temperatures. Based on this result, an active device such as a lid is necessary for small lunar landers to survive lunar nights. In Figure 6.17, the temperature decreases more rapidly in the absence of a lid compared to the absence of RHUs. Therefore, it can be concluded that, for a lunar lander, the effectiveness of a lid is greater than the effectiveness of RHUs for night survival.

For cases with a lid but no RHUs, the difference between the maximum and the minimum temperatures is 80 K, which is greater than the requirement of 70 K of this study. However, the temperature requirement of the lunar lander may potentially be satisfied by efficiently arranging the internal components of an actual lunar lander or by optimizing the radiator area. However, this study could not make conclusions regarding this possibility as the lunar lander was modeled as a simple cube. Instead, a detailed study on this topic is suggested as a future research subject.

6.6 Regolith Temperature Analysis according to the Effect of the MLI Curtain

The temperature of the regolith inside the MLI curtain was compared to the temperature of the external regolith to investigate the heat protection effect of the MLI curtain of the lander on the lunar regolith. The results are presented in Figure 6.18.
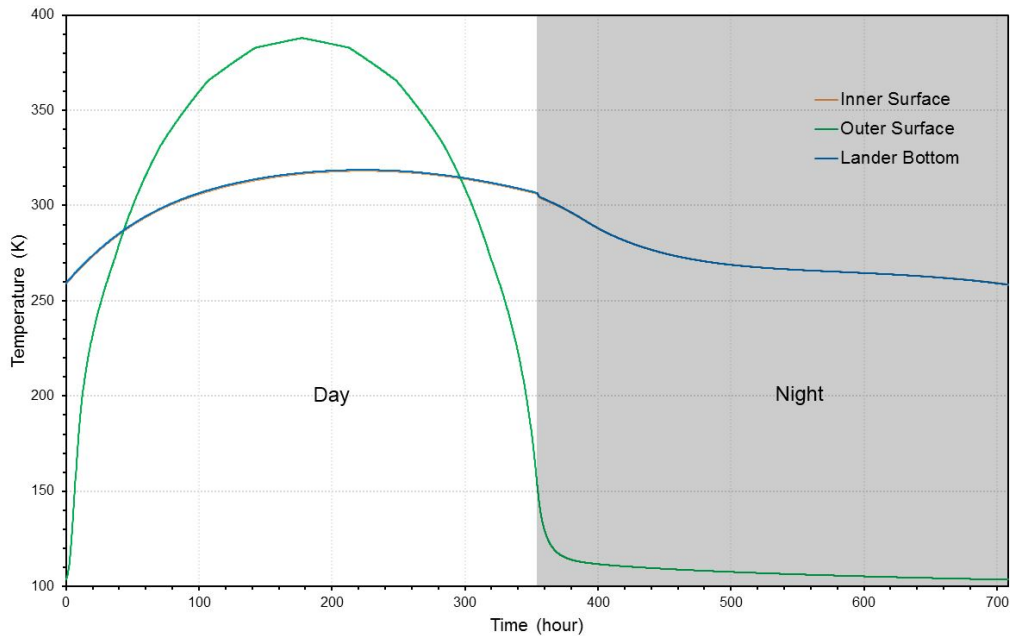
Figure 6.18 Comparison of the temperatures of the inner regolith and the outer regolith

In Figure 6.18, the temperature results of the bottom of the lander and the inner surface regolith were difficult to distinguish, as the temperature results were superimposed. Figure 6.18 shows that the temperature of the outer surface regolith is the same as the regolith temperature result of latitude 0º introduced in Figure 5.5. The temperature of the

inner surface regolith follows the temperature of the bottom of the lander. As the fluff layer of lunar regolith possesses significantly low thermal conductivity and significantly small heat capacity, the temperature of the fluff layer inside the MLI curtain can be estimated to be similar to the temperature of the lander bottom which has a relatively large heat capacity.

Figure 6.18 shows that the surface temperature of the Moon outside the MLI curtain compared to the temperature within the MLI curtain is 71 K higher during the lunar day and 183 K lower during the lunar night. If a rover is forced to survive a lunar night outside the MLI curtain without survival equipment such as RHUs, the temperature of the rover is likely to exceed acceptance temperature requirements due to the harsh temperature conditions of the Moon. The MLI curtain idea is not feasible on planets like Earth, where there is an atmosphere and a surface with varying thermal conductivity and heat capacity depending on location, and is only feasible in a thermal environment like the Moon. As shown in Figure 6.18, the effectiveness of the MLI curtain was demonstrated by the substantial temperature difference between the space outside and inside the MLI curtain.

6.7 Thermal Analysis considering the Fluff Layer being Blown Away

The lunar surface can be divided into a fluff layer and a regolith layer, with the fluff layer having a lower density. Due to the lightness of the fluff layer, a large amount of particles can be scattered even by relatively small impacts. This is indicated in the records of the Apollo program, which stated that dust had settled on the video camera lens during surface activities by the crew, which were wiped off [16].

Propellant release occurs when a lunar lander attempts a soft landing on the lunar surface. In this process, the spraying of the propellant may remove the fluff layer, which causes the regolith layer to be exposed on the surface. This section describes the thermal analysis results that takes into consideration such a case.
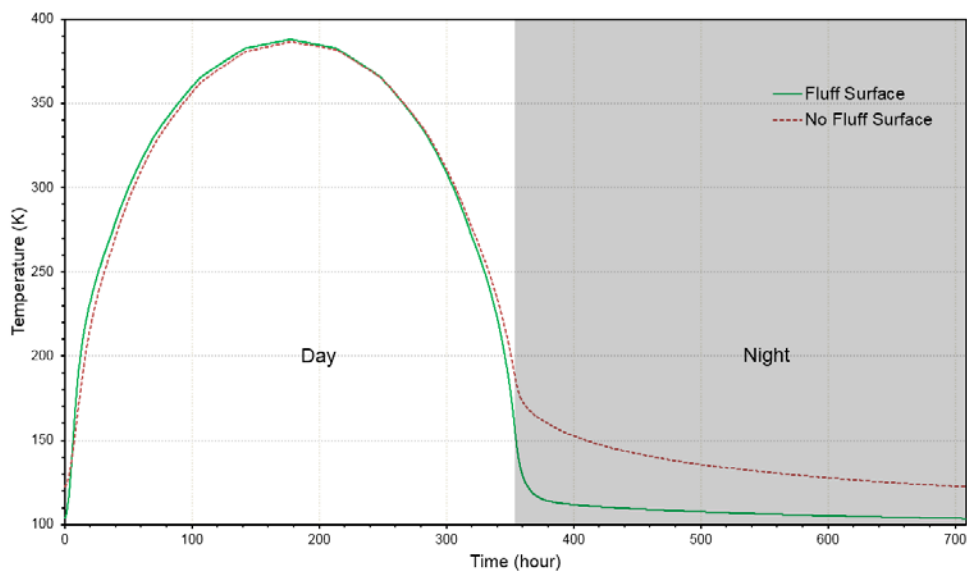
Figure 6.19 Comparison of lunar surface temperature with and without fluff

It is difficult to accurately simulate the shape of fluff layer portions that are blown away from the lunar surface by thrusters. Therefore, the analysis was performed with the assumption that the fluff layer completely disappears in the entire model. The results were compared with the analysis results described in Section 6.4, in which the fluff layer was completely untouched. In Figure 6.19, the temperature results of the lunar surface when the entirety of the fluff layer is removed are compared with the lunar surface temperatures in Figure 5.5.

As shown in Figure 6.19, the highest temperature on the lunar surface is similar in both cases. This is due to the fact that, even when the fluff layer is removed, the maximum temperature due to energy balance remains similar as the model uses the same values for the solar absorptivity and infrared emissivity of the Moon's surface. On the other hand, during the lunar night period, the lowest temperature on the lunar surface exhibits a higher temperature trend when the fluff layer is removed compared to when it is present. This is due to the higher thermal conductivity of the regolith compared to the fluff. Thus, if the fluff is swept away, the temperature of the lunar surface is affected by the temperature below the lunar surface to a greater degree. It is known that the temperature below the lunar surface is higher than the temperature of the lunar surface during lunar nights. Therefore, the removal of the fluff layer is expected to have a positive effect on the survival of a lander and rover due to the smaller gap between the highest and lowest temperatures compared to when the fluff layer is present.

In Figure 6.20, the temperature analysis results of the lander and rover were compared between cases that removed and maintained the fluff layer.
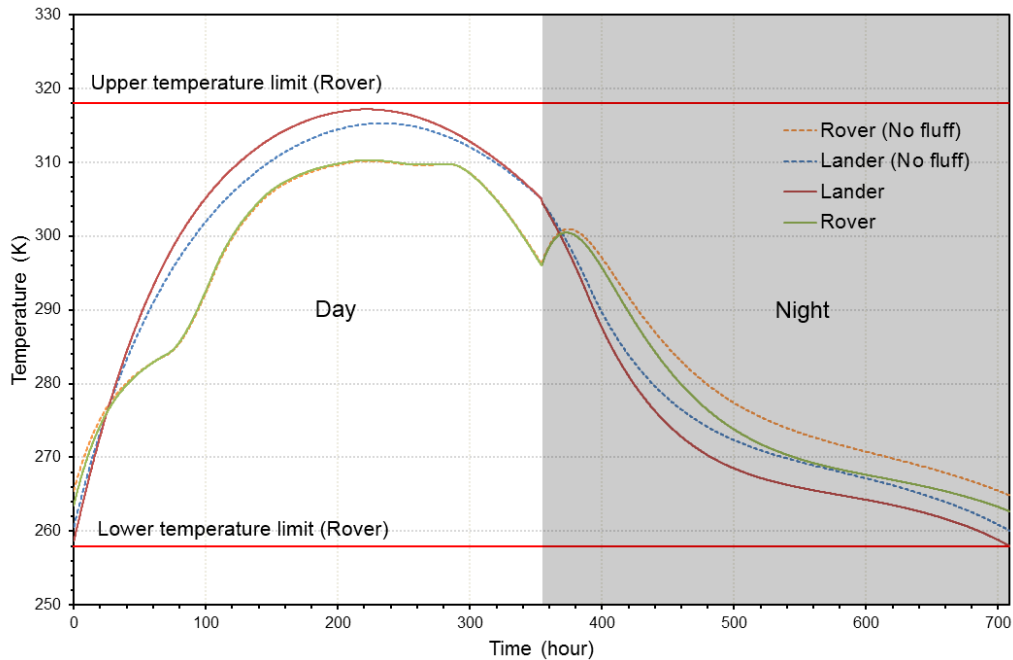
Figure 6.20 Lunar Lander and rover temperatures in cases with and without the fluff

Figure 6.20 shows that the maximum temperatures of the lander and rover were lower in the absence of the fluff layer than with it present. Furthermore, the minimum temperatures of the lander and rover are higher in the former case compared to the latter case. All in all, the lander and rover satisfied their respective allowable temperature requirements in the absence of the fluff layer.

The analysis results of Figure 6.20 are based on the condition of the fluff layer being completely removed by spray thrusters. However, even if the fluff layer is only partially removed, the maximum/minimum temperatures will be lower/higher than if the fluff layer is completely untouched.

From these analysis results, it can be seen that even if the fluff layer is partially or

completely removed by spraying thrusters during the landing process of a lander, thermal

stability does not become an issue for either the lander or rover.

6.8 Summary of Thermal Analysis Results

The analysis results described in Chapter 6 can be summarized as follows. Thermal designing of the lander and rover was undertaken with the goal of satisfying the allowable temperature requirements specified in Table 5.2. As a result, the size of the radiator and the number of RHUs were obtained as shown in Table 6.1.

Thermal analysis of the lander and rover was performed by applying the design results shown in Table 6.1. As a result, it was confirmed that the thermal analysis results of the lander and rover met the allowable temperature requirements and secured appropriate margins, as shown in Figure 6.11 and Figure 6.14. Table 6.2 shows a summary of the results.

Table 6.2 Summary of the Expected Temperatures of the Lander and Rover

	Allowable Temperature Range	Expected Temperature Range	Margin for Min. Temperature	Margin for Max. Temperature
Lander (Average)	-20℃ ~ 50℃	-15℃ ~ 44℃	5℃	6℃
Rover	-15℃ ~ 45℃	-10℃ ~ 37℃	5℃	8℃

As a result of comparing the influence of the lander's RHU and lid for lunar night survival, the role of the lid was confirmed to be greater, as shown in Figure 6.17. In Figure 6.18, the thermal insulation effect of the MLI curtain was confirmed. In addition, in the case of the fluff layer being blown away by thruster propellant, there were no issues in terms of lunar night survival for the lander and rover, as shown in Figure 6.20.

Chapter 7. Conclusions

Survival during night periods on the Moon is a difficult task due to the cryogenic environment, yet it is vital when performing lunar missions for periods of longer than two weeks. Various types of landers and rovers that have landed on the Moon have been thoroughly studied over the years. As a result, long-term missions were identified as difficult tasks for small rovers.

Lunar exploration projects are expensive undertakings, and thus costs are an important factor in the development of space vehicles. In the past, relatively low-cost projects involving lander-rover systems of small masses did not equip the vehicles with adequate means of survival during lunar nights. Therefore, this thesis proposed a cost-effective survival system for lunar landers and small rovers for long-term missions called the MLI curtain system. The system involves a small rover without RHUs that performs mission tasks during the daytime and continues to survive within an MLI curtain shelter under a lunar lander during lunar nights.

This thesis verified the proposed idea through thermal analysis. A lunar regolith thermal model was established and compared with LRO measurement results for verification. A lunar lander thermal model was modeled with a simple cubic shape, and the thermal design combined RHUs and a lid to ensure the lander could survive lunar thermal environments and meet the acceptance temperature requirements. As a result, this study derived the optimized thermal design for a lander to survive lunar days and nights. Furthermore, a thermal model of the MLI curtain and a rover was developed,

103

Chapter 7. Conclusions

which is a key proposal of this study. Using the established thermal model, the lander and rover were thermally designed at 0 ° latitude where the temperature difference between night and day is the most severe, and thermal analysis was performed. Additional thermal analysis was performed to analyze the effectiveness of the RHUs and the lid, and the thermal insulation effect of the MLI curtain was investigated. Furthermore, thermal analysis was performed for the lander and rover for cases in which the fluff layer was blown away by the thrusters during landing. The thermal analysis results showed that the proposed night survival system involving the MLI curtain enables small lunar rovers to survive lunar nights without RHUs or other temperature maintenance devices.

In order to determine the feasibility of the MLI curtain system, we examined its applicability not only in terms of thermal control systems, but also from the perspective of structure mechanical subsystems, electrical power subsystems, and software subsystems. As a result, we were able to confirm a feasible method. In order to improve the feasibility of the MLI curtain system, this thesis suggested methods such as doubled-layer MLI curtains and rovers without solar cells.

In this study, the lunar lander and rover were modeled as simple cubes. Therefore, future research is suggested to verify the details presented in this study using detailed models of lunar landers and rovers that simulate electrical boxes and internal radiation heat exchanges. With further research on rovers that do not equip solar panels and are instead supplied with power solely by lander batteries, lunar exploration missions can be further advanced to widen the scope of lunar research to include lunar night periods.

References

[1] Jose Meseguer, Isabel Perez-Grande and Angel Sanz-Andres, Spacecraft thermal control, 2012, pp. 332.

[2] D. G. Gilmore, Spacecraft Thermal Control Handbook, Volume1: Fundamental Technologies, The Aerospace Corporation, El Segundo, CA, USA, 2nd edition, 2002, pp. 53-55, 143, 241-242, 527.

[3] Yunus A. Cengel, Heat Transfer: A Practical Approach, 2nd edition, McGraw-Hill Higher Education, 2002, pp.29, 566-567, 580, 584, 608.

[4] Charles D. Brown, Elements of Spacecraft Design, Wren Software, Inc., Castle Rock, Colorado, 2002, pp.350-351.

[5] Thermal Desktop User's Manual, Ver 5.8, C & R Technologies, Inc., Boulder, CO, USA, 2017.

[6] SINDA/FLUINT User's Manual, Ver 5.8, C & R Technologies, Inc., Boulder, CO, USA, 2015.

[7] Simon Kassel, "Lunokhod-1 Soviet Lunar Surface Vehicle", Advanced Research Projects Agency, 1971.

[8] Leopold Summerer, "Technical Aspects of Space Nuclear Power Sources VII. Radioisotope Heater Units", European Space Agency, ACT-RPT-2327-RHU, 2006.

References

[9] R. Balasubramaniam, R.S. Wegeng, S.A. Gokoglu, N.H. Suzuki, K.R. Sacksteder, "Analysis of solar-heated thermal wadis to support extended-duration lunar exploration", NASA/TM-2010-216254, 2010.

[10] Hager P. B., "Dynamic Thermal Modeling for Moving Objects on the Moon", Technische Universität München, München, 2013, pp. 49.

[11] Robert J. Christie, David W. Plachta, and Mohammad M. Hasan, "Transient Thermal Model and Analysis of the Lunar Surface and Regolith for Cryogenic Fluid Storage", NASA/TM—2008-215300, Glenn Research Center, Cleveland, Ohio, 2008, pp. 2.

[12] Barbara McKissock, Patricia Loyselle, and Elisa Vogel "Guidelines on Lithium-ion Battery Use in Space Applications", NASA/TM-2009-215751, Glenn Research Center, Cleveland, Ohio, 2009.

[13] ESA Requirements and Standards Division, "Space engineering: Thermal control general requirements", ECSS-E-ST-31C, 2008.

[14] M.G. Langseth et al., "Apollo 15: Preliminary Science Report", NASA SP-289, 1972, Chapter 11.

[15] M.G. Langseth et al., "Apollo 17: Preliminary Science Report", NASA SP-330, 1973, Chapter 9.

[16] James A. McDivitt et al., "Apollo 15: Mission Report", NASA-TM-X-68394, 1971, pp.87.

[17] R. Notsu, H. Nagano, H. Ogawa, "Conceptual verification of lunar long-duration method by using high-heat-storage-capability of regolith", *Journal of Thermophysics and Heat Transfer*, Vol.29, No. 1, 2015, pp. 65-73.

[18] Tae-Yong Park, Jang-Joon Lee, Jung-Hoon Kim, and Hyun-Ung Oh, "Preliminary Thermal Design and Analysis of Lunar Lander for Night Survival", *International Journal of Aerospace Engineering*, Vol. 2018, Article ID 4236396, 2018.

[19] Amitabh, K Suresh, T P Srinivasan, "Potential Landing Sites for Chandrayaan-2 Lander in Southern Hemisphere of Moon", *49th Lunar and Planetary Science Conference*, LPI Contrib. No. 2083, 2018.

[20] Shogo Okishio, Hosei Nagano, Hiroyuki Ogawa, "A proposal and verification of the lunar overnight method by promoting the heat exchange with regolith", *Applied Thermal Engineering*, Vol. 91, 2015, pp.1176-1186.

[21] Gary L.B., James J.L., Richard J.H., Gil S., C.W. Whitemore, Wayne R.A., E.W. Johnson, Alfred S., Roy W.Z., Thomas K.K., James C.H., Richard W.E., " Mission of Daring: The General-Purpose Heat Source Radioisotope Thermoelectric Generator", *4th International Energy Conversion Engineering Conference and Exhibit*, San Diego, California, 2006.

[22] Ashwin R. Vasavada, David A. Paige, Stephen E. Wood, "Near-Surface Temperatures on Mercury and the Moon", *Icarus,* Vol 141*,* Article ID icar.1999.6175, 1999, pp.179-193.

[23] Ashwin R. Vasavada, Joshua L. Bandfield, Benjamin T. Greenhagen, Paul O. Hayne,

References

Matthew A. Siegler, Jean-Pierre Williams, and David A. Paige., "Lunar equatorial surface temperatures and regolith properties from the Diviner Lunar Radiometer Experiment", *Journal of Geophysical Research*, Vol. 117, E00H18, 2012, pp. 1-12.

[24] Williams, J.P., Paige, D.A., Greenhagen, B.T., and Stefan-Nash, E., "The global surface temperatures of the Moon as measured by the Diviner Lunar Radiometer Experiment", *Icarus*, Vol.283, 2017, pp.300-325.

[25] C.K. Krishnaprakas, K. Badari Narayana, Pradip Dutta, "Heat transfer correlations for multilayer insulation systems", *cryogenics*, Vol. 40, 2000, pp.431-435.

[26] M Mirshams, M Samani, and A Darabi, "Cost and mass estimation model of small satellites at system design level.", *5th IAA Symposium on Small Satellites for Earth Observation*, 2005.

[27] Jeffrey L. Linsky, "Models of the lunar surface including temperature-dependent thermal properties", *Icarus*, Vol.5, 1966, pp. 606–634.

[28] S. J. Keihm, and M. G. Langseth, Jr., "Surface brightness temperatures at the Apollo 17 heat flow site: Thermal conductivity of the upper 15 cm of regolith", *Proceedings of the Fourth Lunar Science Conference*, Vol. 3, 1973, pp. 2503–2513.

[29] David L. Mitchell and Imke de Pater, "Microwave imaging of Mercury's thermal emission at wavelengths from 0.3 to 20.5 cm", *Icarus*, Vol. 110, 1994, pp.2–32.

[30] T.Y.Kim, "Lumped System Analysis on the Lunar Surface Temperature Using the Bottom Conductive Heat Flux Model", *J. of The Korean Society for Aeronautical and Space Sciences*, Vol 47, No.1, 2019, pp.66-74.

[31] D.K.Kim, J.H.Choi, J.J.Lee, K.I.Han, T.K.Kim, "Study on view factor calculation for radiative heat transfer by using the mesh subdivision method", *J. of Computational Fluids Engineering*, Vol.19, No.1, 2014, pp.1-6

[32] H.J.Park, W.J.Tak, B.K.Han, D.G.Kwag, J.H.Hwang, B.K.Kim, "Non-explosive Low-shock Separation Device for small satellite", J. of The Korean Society for Aeronautical and Space Sciences, Vol. 37, No 5, 2009, pp.457-463.

[33] Grimm, C.D., Lange, C., Lange, M. et al. The MASCOT separation mechanism. CEAS Space J (2020). https://doi.org/10.1007/s12567-020-00302-y.

[34] Y.I. Yoo, J.W. Jeong, J.H. Lim, K.W. Kim, D.S. Hwang, and J.J. Lee, "Development of a non-explosive release actuator using shape memory alloy wire", *Review of scientific instruments*, Vol. 84, Issue 1, 2013, doi:10.1063/1.4776203.

[35] Hasan, Kazi & Nahid, Abdullah & Reza, Khondker Jahid., "Path planning algorithm development for autonomous vacuum cleaner robots", *2014 International Conference on Informatics, Electronics and Vision, ICIEV*, 2014, doi:10.1109/ICIEV.2014.6850799.

[36] F. Lu, H. Zhang, C. Mi, "A Review on the Recent Development of Capacitive Wireless Power Transfer Technology", *Energies*, 2017, Vol. 10, Issue 11, doi:10.3390/en10111752.

[37] https://nssdc.gsfc.nasa.gov/nmc/SpacecraftQuery.jsp

[38] http://pib.nic.in/newsite/PrintRelease.aspx?relid=183103

References

[39] https://www.nasaspaceflight.com/2019/01/china-returning-moon-change-4-
     mission/

[40] https://www.airspacemag.com/daily-planet/chinas-journey-lunar-far-side-missed-
     opportunity-180963703/

[41] https://www.lpi.usra.edu/sbag/meetings/jan2014/presentations/08_1545_McNutt
     _Pu238_SBAG.pdf

[42] https://www.bobthealien.co.uk/moon/landingsites.htm

[43] https://www.hq.nasa.gov/alsj/LM_Lunar_Module_ppLV1-17.pdf

[44] https://www.qioptiq.com

[45] By de:Benutzer:HPH on "Russia in Space" exhibition (Airport of Frankfurt,
     Germany, 2002), https://commons.wikimedia.org/w/index.php?curid=176704

[46] By Chinese National Space Administration/China Central Television -
     http://www.planetary.org/multimedia/space-images/spacecraft/jade-rabbit-on-the-
     moon.html

[47] https://www.isro.gov.in/chandrayaan2-spacecraft

[48] https://rps.nasa.gov/system/downloadable_items/31_Final_RHU_Fact_Sheet_
     2016_5-26-16.pdf

[49] By Petar Milošević, CC BY-SA 3.0, https://commons.wikimedia.org/w/
     index.php?curid=8361136

[50] Space Engineering Laboratory, Mission Costs and Reliability,
     http://www.yorku.ca/bquine/pages/mission_ costs_and_reliability.htm

[51] By Dantor assumed (based on copyright claims), CC BY-SA 2.5, https://commons.wikimedia.org/w/index.php?curid=1892822

[52] By NASA - http://solarsystem.nasa.gov/rps/rtg.cfm JPG, public domain, https://commons.wikimedia.org/w/index.php?curid=842503

[53] https://www.nasa.gov/centers/johnson/techtransfer/technology/MSC-22379-1-trasys.html

[54] By Peter Sobchak, CC BY-SA 4.0, https://commons.wikimedia.org/w/index.php?curid=35889221

[55] https://tiniaerospace.com/products/space-frangibolt/

[56] https://www.rohm.com/electronics-basics/wireless-charging/wireless-charging-methods

[57] https://moon.nasa.gov/exploration/history/

[58] https://nssdc.gsfc.nasa.gov/nmc/spacecraft/display.action?id=1990-007A

[59] https://nssdc.gsfc.nasa.gov/nmc/spacecraft/display.action?id=2007-039A

[60] https://nssdc.gsfc.nasa.gov/nmc/spacecraft/display.action?id=2003-043C

[61] https://nssdc.gsfc.nasa.gov/nmc/spacecraft/display.action?id=2018-103A

[62] https://nssdc.gsfc.nasa.gov/nmc/spacecraft/display.action?id=2019-042A

초 록

달의 하루는 지구의 한달에 해당하며, 태양이 비치는 달의 2주동안은 매우 뜨거운 상태의 달의 낮기간이고, 태양이 비치지 않는 달의 2주동안은 매우 차가운 달의 밤기간이다. 달 탐사선은 달의 밤기간동안 태양으로부터의 에너지 공급도 없고, 매우 추운 주변 환경 가운데서 2주간의 긴 기간을 버텨야 한다.

달 탐사를 위한 착륙선과 로버에는 2주동안의 달의 밤기간동안 생존하기 위해 그동안 여러가지 장치가 제안되고 시도되어 왔다. 달의 밤기간동안 달 탐사선의 열 공급장치인 RHU(Radioisotope Heating Unit), 혹은 전기 발생장치인 RTG(Radioisotope Thermoelectric Generator)등이 사용되어 왔고, 열 개폐장치인 Radiator Lid등이 사용되었다. 최근에는 열 저장 장치인 Thermal Wadi나 달의 지표면 아래에 달의 낮기간 동안 에너지를 저장하는 장치 등의 아이디어도 제시되었다.

이와 같은 온도 유지장치들은 가격적인 문제나 안전문제 혹은 무게나 구현의 어려움 등의 문제점을 동반하기 때문에, 소형 달탐사선의 경우에는 달 밤 기간 동안의 생존을 포기하고 달의 낮 기간인 2주동안만을 임무기간으로 설계되어 제작되기도 하였다.

본 논문에서는 소형 달착륙선과 로버도 2주동안의 달의 밤기간동안 생

존할 수 있는 아이디어를 제시하였는데, 그것은 MLI (Multi-Layer Insulation) curtain system이다. MLI curtain system은 달 착륙선에 Lid와 RHU등의 장치를 적용하여 달의 밤 기간 동안 생존할 수 있도록 하고, 달 탐사 로버는 달 착륙선의 MLI curtain 안의 shelter로 이동하여 생존할 수 있도록 설계된 시스템이다. MLI curtain system은 소형 로버의 달 밤 기간 생존을 위하여 그 아이디어가 간단하고 적은 비용으로도 구현할 수 있는 장점을 갖는다.

본 논문에서는 MLI curtain system의 실현 가능성을 증명하기 위해 일반적인 우주비행체 열설계 열해석 과정을 따라 열설계와 열해석을 수행하였고, 열설계 요구조건에 부합하는 결과물을 얻었다. 뿐만 아니라 MLI curtain system feasibility를 향상시키기 위해 열제어 뿐만 아니라 구조, 전력, 소프트웨어 측면에서 고려할 점도 논하였으며, MLI curtain system의 안정성을 향상시키기 위한 아이디어도 제시하였다. 그 결과 MLI curtain system은 소형 로버의 긴 임무기간 동안의 생존을 위해 실현 가능하고 적합한 아이디어임을 증명할 수 있었다.